Agricultural and Forest Meteorology 386 (2026) 111225

Contents lists available at ScienceDirect

Agricultural and Forest Meteorology

journal homepage: www.elsevier.com/locate/agrformet

Lowland tropical forests remain a methane sink under warming and long-term hurricane disturbance recovery

Gabriele Larocca Conte [a,*], Lucia Zuvela [b], Rachel Cruz-Pérez [c], Tatiana Barreto-Vélez [d], Nibia Becerra-Santillan [e,f], Sophia F. Campbell [g], Hieu P. Chu [f], Trung Dam [b,f], Iana F. Grullón-Penkova [d], Miriam Kleit [e], Deyaneira A. Ortiz-Iglesias [d], Laura C. Rubio-Lebrón [d], Molly A. Cavaleri [h], Sasha C. Reed [i], Debjani Sihi [j], Tana E. Wood [d], Christine S. O'Connell [a,b,*]

[a] Department of Biology, Schmid College of Science and Technology, Chapman University, 1 University Dr, Orange, CA 92866, United States
[b] Department of Environmental Studies, Macalester College, 1600 Grand Ave, St Paul, MN 55105, United States
[c] Department of Ecosystem Science and Management, Pennsylvania State University, 453 Shortlidge Rd, University Park, PA 16802, United States
[d] U.S.D.A. Forest Service, International Institute of Tropical Forestry, Río Piedras, Jardin Botanico Sur, 1201 C. Ceiba, San Juan, 00926, Puerto Rico, United States
[e] Department of Biology, Macalester College, 1600 Grand Ave, St Paul, MN 55105, United States
[f] Department of Math, Stats and Computer Science, Macalester College, 1600 Grand Ave, St Paul, MN 55105, United States
[g] Geological Sciences Program, George Washington University, 2121 I St NW, Washington, DC 20052, United States
[h] College of Forest Resources and Environmental Science, Michigan Technological University, 1400 Townsend Dr., Houghton, MI 49931, United States
[i] U.S. Geological Survey, Southwest Biological Science Center, 2290 SW Resource Blvd Moab, UT 84532, United States
[j] Departments of Plant and Microbial Biology and Crop and Soil Sciences, N.C. Plant Sciences Initiative, North Carolina State University, Raleigh, NC 27695, United States

ARTICLE INFO

Keywords:
Methane
Tropical forests
Warming
Experimental manipulation
Climate change
Soil respiration

ABSTRACT

Methane (CH_4) is a potent greenhouse gas, and tropical forests account for roughly one–third of global atmospheric CH_4 uptake by soils. Projected warming and more frequent hurricanes in these ecosystems may alter soil CH_4 sink strength, as warmer and wetter soils enhance methanogenesis activity. We measured soil CH_4 and CO_2 efflux during the calendar summer months of 2023 and 2024 alongside continuous records of soil moisture, soil and air temperature, and precipitation in an *in–situ* warming experiment (TRACE) located in a lowland tropical forest in Puerto Rico, six to seven years after Hurricanes Irma and Maria (2017). The realized warming (~1.95°C) enhanced soil respiration only in summer 2023 ($p < 0.05$), but net soil CH_4 uptake was invariant in both campaigns ($p > 0.05$). Instead, sampling day and between–plot variability explained soil CH_4 dynamics much more than treatment contrasts. Importantly, CH_4 uptake was consistently coupled to CO_2 efflux, suggesting tight linkages between methanotrophic and heterotrophic activities. Between treatments, CH_4 and CO_2 responses to soil temperature variation were less sensitive in warmed plots, which may suggest weak metabolic upregulation under elevated temperatures. Together, these findings indicate that lowland tropical soils remain CH_4 sink even under warming and years after hurricane disturbance, with CH_4 dynamics driven more by spatial and temporal variability than experimental warming. Long–term, high–resolution monitoring integrating soil biogeochemistry and microbial processes will be critical to determine whether the observed net CH_4 uptake signal represents a sustainable or transient response under continued warming and disturbance.

Abbreviations: AIC, Akaike Information Criterion; BIC, Bayesian Information Criterion; C, carbon; CH_4, methane; CI, confidence interval; CO_2, carbon dioxide; df, degrees of freedom; $\Delta T_{Warming\text{-}Control}$, soil temperature difference between Warming and Control treatments; $\Delta VWC_{Warming\text{-}Control}$, soil moisture difference between Warming and Control treatments; GAMM, Generalized Additive Mixed Model; IR, infrared; LEF, Luquillo Experimental Forest; LLM, linear mixed-effect model; N, nitrogen; NO_3^-, nitrate; ppm, parts per million; QC, quality control; Q-Q plot, quantile-quantile plot; REML, Restricted Maximum Likelihood; SE, standard error, soil GHG, soil greenhouse gases; soil T, soil temperature; TRACE, Tropical Responses to Altered Climate Experiment; VWC, volumetric water content (soil moisture).

* Corresponding authors.
E-mail addresses: laroccaconte@chapman.edu (G. Larocca Conte), coconn@chapman.edu (C.S. O'Connell).

https://doi.org/10.1016/j.agrformet.2026.111225
Received 16 November 2025; Received in revised form 29 April 2026; Accepted 1 May 2026
Available online 23 May 2026

1. Introduction

Methane is a potent greenhouse gas (GHG) that absorbs Earth's emitted infrared radiation more efficiently than carbon dioxide (CO_2), with a global warming potential approximately 28 times greater over a 100-year time horizon (Saunois et al., 2025, 2020). Since 1750, atmospheric methane (CH_4) concentrations have nearly tripled, reaching ~1.934 parts per million (ppm) as of April 2025 (Lan et al., 2025). This increase is largely driven by anthropogenic activities, such as fossil fuel extraction, livestock production, and rice cultivation, which emit approximately 369 Tg CH_4 per year and account for an estimated ~31% of historical global warming since pre-industrial times (Saunois et al., 2025, 2020). Soils can play a substantial role in terrestrial exchange of CH_4 with the atmosphere, including through the microbial production of CH_4 via methanogenesis (methane emission/source). At the same time, other microbes in soils consume CH_4 (i.e., via methanotrophy, methane uptake/sink), and the net exchange of CH_4 between soils and the atmosphere is determined by the balance in microbial processing that produces versus consumes CH_4 (Nazaries et al., 2013; O'Connell et al., 2018; Silver et al., 2013; Zhao et al., 2019). Although CH_4 has a relatively short atmospheric lifetime (~9 years), natural removal processes may not be keeping pace with rising emissions (Collins et al., 2013; Nisbet et al., 2019). Microbial consumption of CH_4 in soils represents the only terrestrial biogeochemical sink for atmospheric methane, removing ~7% of atmospheric CH_4 (Dutaur and Verchot, 2007; Saunois et al., 2025, 2020). Thus, monitoring soil net CH_4 flux rates can support improved accuracy of future climate predictions, and uncertainties persist in how soil CH_4 flux rates may change alongside shifting climate and disturbance regimes.

Among terrestrial biomes, tropical forests play a disproportionate role in global carbon (C) cycling (Bonan, 2008; Chambers et al., 2004; Malhi and Grace, 2000; Pan et al., 2011), accounting for approximately 31% of global atmospheric CH_4 uptake (~9-49 Tg CH_4 y^{-1}) (Dutaur and Verchot, 2007; Saunois et al., 2025, 2020; Zhuang et al., 2013). Yet under a warmer climate, the strength of the tropical soils CH_4 sink may be altered, with some studies suggesting conditions under which net CH_4 emissions could increase, exacerbating radiative forcing (Feng et al., 2022; O'Connell et al., 2018; Quebbeman et al., 2022a). Projected warming of up to ~4°C in tropical latitudes (IPCC, 2018) is expected to interact with other climate-driven disturbances, notably the increasing frequency and intensity of tropical cyclones (i.e., hurricanes) (Knutson et al., 2019). Forest recovery from a hurricane can trigger long–term shifts in soils and microbial communities that persist for years after disturbance, compounding the warming effect (Reed et al., 2020; Townsend et al., 2011). The diversity of climates, precipitation regimes, and biodiversity across tropical forests (Townsend et al., 2008) further complicates the assumption of a uniform response of these ecosystems to global warming (McFarlane et al., 2024; Nottingham et al., 2015). An Earth System Model intercomparison found that projected C balance in tropical regions shows three times more variability than in any other latitude band, highlighting persistent challenges in representing C dynamics in these C-rich ecosystems (Cavaleri et al., 2015). Indeed, even subtle shifts in tropical forest C cycling under warmer conditions could have substantial implications for methane emissions and their feedback to global climate.

The two opposing microbial fluxes that determine net CH_4 efflux in tropical soils are regulated by the availability of oxygen, with methanogenesis occurring under anaerobic conditions, and methanotrophy under aerobic condition (Nazaries et al., 2013; O'Connell et al., 2018; Silver et al., 2013; Zhao et al., 2019). In tropical forests, deeper soil layers are often saturated and poorly oxygenated, favoring methanogenesis, whereas upper mineral horizons are typically well–aerated, allowing methanotrophs to oxidize CH_4 into CO_2 from both upward diffusion of microbially produced methane and downward diffusion of atmospheric methane at the soil–atmosphere interface (Dijkstra et al., 2011; Dutaur and Verchot, 2007; Zhao et al., 2019). Soil aeration, and therefore redox status, is largely controlled by soil moisture content. Higher soil moisture reduces air–filled pore space, creating anoxic conditions that promote methanogenesis. Conversely, drier soils generally favor methanotrophy, although activity declines if moisture levels fall below the methanotrophs' physiological optimum (Castro et al., 1995; Dijkstra et al., 2011; Nazaries et al., 2013; Voigt et al., 2023; Wanyama et al., 2019; Zhao et al., 2019). In the context of climate warming and post–hurricane recovery, shifts in soil moisture and aeration can persist for years, potentially reshaping microbial redox environments and regulating whether tropical soils act as stronger or weaker CH_4 sinks.

Soil temperature also may modulate methanotrophic activity directly by increasing metabolic rates, or indirectly by enhancing aeration and drying (Castro et al., 1995; Wu et al., 2010). Under warming alone, higher temperatures and reduced soil moisture are generally expected to strengthen the CH_4 sink (Dijkstra et al., 2011; D'Imperio et al., 2017; Peltoniemi et al., 2016). Warming often reduces methanogen abundance (Peltoniemi et al., 2016), while the remaining microbes, potentially methanotrophs, respond rapidly, potentially competing with plants for nutrients (Reed et al., 2020). This shift can increase microbial biomass pools (Reed et al., 2020) and respiration rates (Kirschbaum, 2006; Wood et al., 2025), while suppressing methane production (Peltoniemi et al., 2016). These combined processes frequently produce a negative correlation between CH_4 and soil respiration (i.e., soil CO_2 efflux), where enhanced CH_4 uptake coincides with elevated CO_2 emissions (Voigt et al., 2023; Zhao et al., 2019). However, in combination with hurricane disturbance, the response can differ (Reed et al., 2020).

When hurricanes strike, they substantially alter both above– and belowground biomass, triggering cascading effects on biogeochemical cycles (Frangi and Lugo, 1991; Lodge et al., 1991; Scatena and Larsen, 1991; Steudler et al., 1991). Intense storms strip leaves and branches from canopy trees, transferring large amounts of biomass to the soil, altering light availability, and modifying the understory microclimate until the canopy recovers (Shiels et al., 2014). Root biomass is also reduced after hurricanes (Tunison et al., 2024). These structural changes result in higher soil moisture likely due to reduced plant evapotranspiration and greater throughfall (Reed et al., 2020; Shiels et al., 2014; Steudler et al., 1991), while also increasing nutrient inputs from decomposing litter and roots (Frangi and Lugo, 1991; Lodge et al., 1991; Reed et al., 2020; Tunison et al., 2024; Yaffar et al., 2021). Enhanced litterfall inputs under wetter conditions sustain nutrient–rich environments that stimulate shifts in soil microbial community structure, resulting in lower richness but higher abundance of taxa adapted to such conditions, including methanogens (Eaton et al., 2020; Finn et al., 2020; Lodge et al., 1991). A recent study suggests that such post–hurricane nutrient pulses can shift soils from a CH_4 sink to a net source, accompanied by elevated CO_2 efflux (Quebbeman et al., 2022a). One mechanism is the enhanced decomposition of low–quality substrates such as pectin and lignin into acetate (Corteselli et al., 2017), a preferred substrate for methanogens in water–saturated tropical soils (Sihi et al., 2021). Acetoclastic methanogenesis (i.e., acetate conversion to CH_4) also releases CO_2 as a byproduct (Conrad, 2020), which may explain any observed concurrent rise in CO_2 and CH_4 fluxes after hurricanes. When hurricane impacts occur in ecosystems already "stressed" by prior warming, the combined effects can fundamentally alter soil biogeochemical cycling and ecosystem resilience (Reed et al., 2020). This warming–hurricane interaction may produce a second legacy effect, where the prior thermal stress modifies the post–disturbance trajectory of soils and microbial communities for years after the tropical cyclone/storm (Reed et al., 2020; Townsend et al., 2011; Yaffar et al., 2021), potentially amplifying soil GHG emissions. Under altered soil moisture, redox conditions, and nutrient inputs supplied by hurricane disturbance, warming may accelerate decomposition and substrate supply for methanogenesis (Wilson et al., 2021), tipping soils toward greater CH_4 and CO_2 emissions. Such changes may influence soil GHG fluxes well beyond the immediate disturbance period, persisting until canopy structure, and consequently throughfall and evapotranspiration, recovers toward pre–hurricane stages (Shiels et al., 2014; Quebbeman et al., 2022b). Although aboveground canopy cover can recover within ~24 months, hurricane–derived canopy debris and altered soil structure can persist for several years (>4 years; Shiels et al., 2014), sustaining elevated soil moisture and modified redox conditions during ecosystem recovery. Under these legacy conditions, sustained warming does not act independently, but rather may modulate hurricane–driven changes in soil moisture and microbial environments, influencing whether soils function as net CH_4 sinks or sources. These interactive effects are expected to be strongest during warmer and wetter periods of the year (e.g., the calendar summer months), when elevated air temperatures (González et al., 2025) and rainfall (García-Martinó et al., 1996) further increase soil temperature and maintain high soil moisture, with evaporation buffered by persistent debris layers accumulated following hurricane events (Shiels et al., 2014). In this context, warming may amplify hurricane legacy effects by increasing the likelihood of seasonal shifts toward net CH_4 emissions. Whether such seasonal shifts from net sink to source occur and persist in a warmer world remains unclear, a knowledge gap that could obscure unexpected ecosystem trajectories and bias global CH_4 budget estimates in climate models.

To address this gap, we conducted a field–based observational study of soil CH_4 and CO_2 fluxes in the wake of both >5 years of ecosystem warming and recovery from a large–scale hurricane disturbance in a wet tropical forest. This study was conducted at the Tropical Responses to Altered Climate Experiment (TRACE) in Puerto Rico, a unique long–term warming manipulation in a lowland tropical ecosystem. The TRACE site has undergone multiple years of experimental warming both before and after Hurricanes Irma and Maria struck on September 6 and 20, 2017, respectively (Kimball et al., 2018; Reed et al., 2020; Tunison et al., 2024; Yaffar et al., 2021). We present a targeted study examining the mechanistic responses of soil methane fluxes to altered abiotic conditions, specifically soil temperature and moisture, and evaluate soil CO_2 efflux as a proxy for microbial activity and decomposition turnover rates following prolonged warming and several years of hurricane recovery, compared to unwarmed plots (i.e., Control) during the summer months of 2023 and 2024.

Previous studies at TRACE have examined soil biogeochemistry (Reed et al., 2020), root dynamics (Tunison et al., 2024), and soil respiration (Wood et al., 2025) under the combined legacy effects of warming and Hurricanes Irma and Maria. However, the directional response of soil CH_4 fluxes under the same treatments and legacy effects remained unexplored. Here, we explicitly investigated soil CH_4 dynamics at TRACE under the dual, interactive legacies of prolonged warming and ecosystem recovery from hurricane disturbance, a context not previously explored at this site. Based on the integration of soil CH_4 flux responses to variation in abiotic conditions and heterotrophic activity, we tested two contrasting hypotheses regarding whether lowland tropical soils act as a CH_4 sink or source under warmer conditions following hurricane disturbance:

Hypothesis 1. Under this scenario, sustained warming attenuates hurricane legacy effects by enhancing soil aeration following ecosystem recovery. Warming–induced drying and increased soil aeration promote methanotrophic activity and suppress methanogenesis, resulting in soils functioning more as a net CH_4 sink. We expect warming to generate drier conditions and higher CH_4 uptake (i.e., more negative CH_4 fluxes), accompanied by elevated soil CO_2 efflux indicative of increased microbial respiration. The observed negative correlation between soil CH_4 and CO_2 effluxes may arise from two, not mutually exclusive mechanisms: (*i*) favorable warmer and drier soil conditions that concurrently stimulate methanotrophs and other heterotrophs, and/or (*ii*) direct biological coupling through the oxidation of CH_4 to CO_2 by methanotrophs under altered conditions.

Hypothesis 2. Alternatively, sustained warming may amplify long–term hurricane legacy effects, reducing soil CH_4 strength toward net methane emission. In combination with nutrient pulses from canopy–derived litter and altered hydrology associated with long–term storm impacts, wetter soil conditions combined to accelerated warming–driven could enhance anaerobic methanogenesis and shift soils from a CH_4 sink to a net source. Under this scenario, we expect warming to increase CH_4 emissions while also elevating CO_2 efflux through stimulated microbial turnover under persistently high soil moisture conditions.

2. Materials and methods

2.1. Site description

This research was conducted from June 2023 to July 2024 at the Tropical Responses to Altered Climate Experiment (TRACE) site, located next to the Sabana Field Research Station within the Luquillo Experimental Forest (LEF, El Yunque National Forest, USDA Forest Service; 18°19′28.74″ N, 65°43′50.09″ W; Fig. 1) in Puerto Rico at an elevation of ~122 m a.s.l. The site hosts a unique subtropical wet forest (Holdridge, 1967) characterized by a mean annual temperature of approximately 24 °C and a mean annual precipitation of about 3,500 mm, based on records from 1970 to 1994 (García-Martinó et al., 1996). Mean diurnal and monthly temperatures experienced in this forest are narrow, ranging from 20 to 26°C (Wood et al., 2025) and 23.5 to 27°C (García-Martinó et al., 1996), respectively. Although there is no pronounced dry season in this rainforest, the driest period typically occurs between January and March, when monthly precipitation drops below 200 mm and exhibits lower variability compared to the rest of the year (Heartsill-Scalley et al., 2007). Given the documented variability in magnitude and temporal distribution of rainfall across tropical latitudes in recent decades (Feng et al., 2013; O'Connell et al., 2018), we intentionally refrained from using climatologically confounding terminology to define seasonal boundaries associated with calendar conventions, especially in a weakly seasonal system like Puerto Rico. Accordingly, conventional calendar seasons, such as "summer", are used solely as temporal descriptors to distinguish sampling campaigns, without implying specific climatological states. While the TRACE site may experience periods of higher rainfall, these wetter conditions are probabilistically distributed across multiple months, including, but not limited to, those corresponding to calendar summer (García-Martinó et al., 1996; Heartsill-Scalley et al., 2007).

2.2. Experimental design

The TRACE plot array consists of six *in-situ* hexagonal replicates selected to represent similar soil composition and understory vegetation while accounting for topographic variability. Soils at the site are acidic and clay–rich, classified as Oxisols originating from volcanoclastic parental material (Beinroth et al., 2003; Muñoz et al., 2018). Understory vegetation within each plot is generally dominated by *Psychotria brachiata, Piper glabrescens, Guarea guidonia, Miconia racemosa, Inga vera*, and *Prestoea acuminata* (Tunison et al., 2024). All plots are situated on slopes ranging from 18° to 26° (Kimball et al., 2018).

Three of the six 12 m^2 plots are actively warmed using rectangular infrared (IR) heaters mounted on galvanized steel posts (i.e., Warming treatment). The warming manipulation experiment was initiated on September 28, 2016, but was interrupted almost one year later (September 5, 2017) due to Hurricanes Irma and Maria (Reed et al., 2020). The storms caused severe canopy disturbance and widespread damage to the island's power infrastructure, as well as portions of the heating and plot infrastructure at TRACE. The warming system was repaired in July 2018 and resumed operation in September 2018 (Tunison et al., 2024). To accommodate post–hurricane understory plant growth, the heaters were initially positioned 1–2 m above the

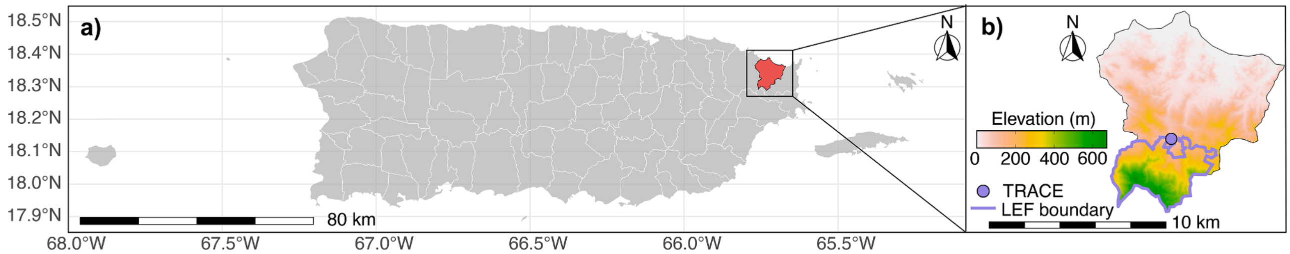

Fig. 1. Location of the Tropical Responses to Altered Climate Experiment (TRACE) site. **a)** Map of Puerto Rico showing municipal boundaries in white; Luquillo municipality is highlighted in red. **b)** Zoom-in of Luquillo municipality with the TRACE site marked by a dark indigo point (18°19′28.74″ N, 65°43′50.09″ W). The basemap layers were created with shape files from the U.S. Census Bureau (https://www.census.gov/geographies/mapping-files/time-series/geo/tiger-line-file.html). The dark indigo outline marks the Luquillo Experimental Forest (LEF) boundary, adapted from the Luquillo Critical Zone Observatory dataset (Gould et al., 2018). Elevation is displayed using a continuous white-to-green gradient, from low to high values, highlighting the lowland position of the TRACE subtropical forest site at 122.07 m a.s.l., calculated with the *elevatr* package (Hollister et al., 2023).

understory vegetation (Kimball et al., 2018), then raised to 2.5 m after the hurricanes, and subsequently elevated to a maximum height of 4 m beginning in July 2020. The remaining three plots, constructed identically but left unwarmed, serve as ambient controls to assess treatment effects on soil and ecosystem responses (i.e., Control treatment). More details about IR–system operation and design are found in Kimball et al. (2018). Finally, soil GHG measurement campaigns were conducted during the summer campaigns of 2023 (June–August) and 2024

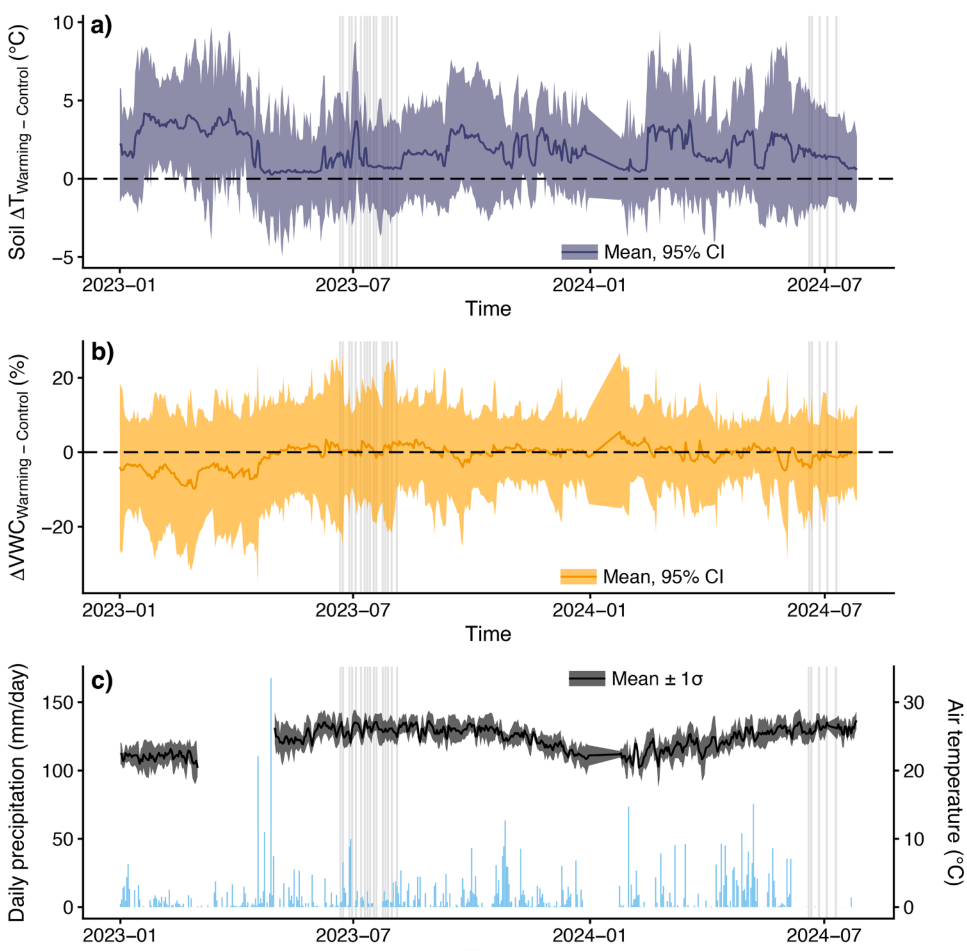

Fig. 2. Soil temperature and moisture differences between Warming and Control treatments at the Tropical Responses to Altered Climate Experiment (TRACE) site, Puerto Rico, were largely influenced by seasonal and daily variation in air temperature and precipitation from January 2023 to July 2024. Soil measurements at 0–10 cm depth, aggregated by sensor location within plots, were used to calculate differences in soil abiotic variables between treatments. Vertical grey bars in each panel indicate the days during which soil greenhouse gas (GHG) measurements were taken. **a)** Time series of soil temperature differences between Warming and Control plots (Soil $\Delta T_{Warming-Control}$; °C). Violet lines represent mean daily differences averaged by plot; shaded areas show the 95% confidence interval (CI). **b)** Time series of soil moisture differences between Warming and Control plots (Soil $\Delta VWC_{Warming-Control}$; VWC = volumetric water content). Yellow lines represent mean daily differences averaged by plot; shaded areas show the 95% CI. **c)** Daily precipitation (light blue bars) and mean ±1σ air temperature (line and shaded area). Precipitation data were downloaded from the publicly available Sabana Tower station dataset (González et al., 2025). The horizontal dashed line at 0% and 0°C in panels **a)** and **b)** separates positive from negative differences in soil moisture and temperature, respectively.

(June–July), approximately four years after TRACE facility resumed operation and more than five years after the hurricane events.

Each IR–warmed plot is paired with a Control plot of similar topographic position and slopes (Kimball et al., 2018; Reed et al., 2020; Tunison et al., 2024; Wood et al., 2025). Warmed plots are independently and continuously controlled to maintain an average soil temperature increase of approximately 4 °C relative to the average ambient temperature in control plots (Kimball et al., 2018). To assess treatment consistency and environmental variation, air temperature, soil temperature, soil moisture, and precipitation were continuously monitored during the study period.

Each plot was instrumented with Campbell CS655 soil moisture (Volumetric Water Content, VWC) and temperature (Soil Temperature, Soil T) probes (Campbell Scientific, Logan, Utah, USA) installed at the center, at the edge, and midway between these two locations. Each sensor recorded hourly measurements at different depth ranges (0–10, 20–30, and 40–50 cm). All analyses in this study used soil temperature and moisture data measured within 10 cm depth by sensors located at all locations to account for overall soil abiotic conditions within each plot (see Sections 2.3 and 2.4). Data from the same sensors at deeper depths are available for download in the ESS-DIVE database (see Data Availability section).

Soil temperature and moisture differences between treatments were monitored from January 2023 to July 2024. Soil temperature differences between treatments aggregated by plots and day within the upper 10 cm of soil resulted in a mean realized warming effect of 1.95°C (95% CI = 1.10, 2.80°C) (see also Section 2.4, Fig. 2, Table 1, Table SM1). Prior to Hurricane Irma and Maria events, the IR heaters maintained an averaged soil temperature increase of ~3.6°C within the same soil depth range (Kimball et al., 2018). Following the hurricanes, tree trunks and large branches were removed from plots before reinitiating the warming experiment, whereas leaf litter and small woody debris (≤3 cm diameter) were left in place (Reed et al., 2020; Tunison et al., 2024). Since then, the realized soil warming effect declined to ~1°C within the upper 10 cm of soil (Reed et al., 2020; Tunison et al., 2024). To account for this discrepancy between target and achieved warming, all statistical analyses (see Section 2.4 and Section 3) were based on realized soil temperature differences rather than the nominal treatment assignment of +4°C (Kimball et al., 2018), consistent with previous TRACE studies that assess the interactive legacy effects of warming and hurricane recovery (Reed et al., 2020; Tunison et al., 2024).

Table 1
Linear mixed-effects models for soil abiotic variables measured within 10 cm depth from January 2023 to July 2024. Separate models were fitted for soil temperature (a) and soil moisture (b), with Treatment (Warming vs. Control) as a fixed effect. Temporal and spatial dependencies were accounted for by including day and plot as random effects, capturing repeated measurements over time and across plots. Fixed effect estimates are reported with their standard error (SE), degrees of freedom (df), t-values (t), and *p*-values (*p*), and 95% confidence interval (95% CI). The asterisks denote levels of statistical significance: $p < 0.05$ (*), $p < 0.01$ (**), and $p < 0.001$ (***). Random effects report the variance and standard deviation (1σ) of the intercepts across plots and/or days, reflecting the variability in baseline values not explained by the fixed effects. The residual variance and standard deviation represent within-group variability unexplained by the fixed or random effects (i.e., the remaining scatter around the fitted values).

Linear Mixed-Effects Models on Soil Abiotic Variables						
a) Soil Temperature						
Fixed effects	**Parameter**	**SE**	**df**	***t***	***p***	**95% CI**
Control	24.09	0.23	4.82	106.51	2.57E-09***	[25.31, 24.68]
Warming	1.95	0.31	4	5.29	3.10E-03**	[1.10, 2.80]
Random effects	**Term**	**Variance**	**1σ**			
Time (day)	Intercept	2.48	1.57			
Plot	Intercept	0.14	0.37			
Residual	-	1.87	1.37			
b) Soil Moisture (VWC)						
Fixed effects	**Parameter**	**SE**	**df**	***t***	***p***	**95% CI**
Control	0.35	0.01	4.49	29.99	2.38E-06***	[0.32, 0.38]
Warming	-0.01	0.02	4.01	-0.62	0.57	[-0.05, 0.03]
Random effects	**Term**	**Variance**	**1σ**			
Time (day)	Intercept	4.16E-03	0.06			
Plot	Intercept	3.89E-04	0.02			
Residual	-	2.56E-03	0.05			

Air temperature was measured in each plot using a HOBO MX23O1A temperature and relative humidity data logger (Onset Computer Corporation, Bourne, Massachusetts, USA), mounted at a height of 170–240 cm above ground. Hourly precipitation data were obtained from a nearby weather tower at the Sabana Field Research Station and accessed as a public dataset (González et al., 2025).

2.3. Soil GHG measurements

Soil GHG flux measurements were taken during two discrete summer campaigns in 2023 and 2024. In summer 2023, data collection began on June 21, and measurements were taken intermittently until August 4, 2023. The campaign resumed in 2024, with data collection occurring between June 19 and July 10. Soil GHG flux sampling occurred at irregular intervals, with gaps ranging from two to seven days between field sampling days across all plots. In total, the GHG measurement campaign produced a 21–day time series across the summers of 2023 and 2024. The field campaign resulted in a total of 245 measurements of soil GHG fluxes (CH_4 and CO_2). All measurements were taken between 9:00 am and 12:30 pm. Previous studies in tropical forests have shown that soil GHG fluxes exhibit minimal (de Gerenyu et al., 2011; Zhao et al., 2019) or no diurnal variability (Yang et al., 2017). Accordingly, flux measurements collected during the morning window (approximately 08:00–12:00) can be used as proxies for daily mean soil respiration and CH_4 effluxes. Although our measurements do not resolve full diurnal cycles, this sampling window provides a reasonable approximation of mean daily soil GHG fluxes for the purposes of treatment comparisons.

Soil GHG fluxes were measured using two PVC collars per plot (12 collars total): one located near the center, and one located in the middle portion of each plot. All collars were positioned near soil temperature and moisture sensors Campbell CS655. Additionally, collars were distributed avoiding obvious obstructions (e.g., trees, roots). Half of the collars were installed in 2016 (collars L7, M7, L8, M9, U8 and U7 in plot 1–6, respectively) and the other half in 2022 (collars L6, M6, L9, M9, U9, U6 in plot 1–6, respectively) to capture spatial and temporal variability in soil respiration and CH_4 fluxes under warming conditions. Once installed, collars were not moved or relocated. Measurements were conducted using a LI-COR 8200-01S Portable Smart Chamber coupled with a LI-COR LI-7810 CH_4/CO_2/H_2O Trace Gas Analyzer (LI-COR, Lincoln, Nevada, USA). For each measurement, the Smart Chamber recorded GHG concentrations over a two-minute flux period, with each collar sampled once daily during the field campaign. The Smart Chamber also recorded relative humidity, instrument temperature, and pressure.

Soil GHG measurements were calculated on SoilFluxPro™ v5.3 Software (LI-COR, Lincoln, Nevada, USA). For each measurement, both linear and exponential models were applied to dilution-corrected gas concentrations, using automated slope cutoffs to optimize model fit based on R^2 values.

2.4. Data analysis

We developed a data analysis framework that integrates measurements of soil abiotic conditions (i.e., temperature and moisture within 0–10 cm depth) and soil GHG fluxes to evaluate the response of soil respiration and methane emissions to experimental warming at the TRACE site. To observe treatment effects on soil moisture and temperature, we calculated daily differences in soil moisture (i.e., $\Delta VWC_{Warming\text{-}Control}$) and temperature (Soil $\Delta T_{Warming\text{-}Control}$) between warmed and control plot replicates from January 2023 to July 2024. To account for within–plot variability, particularly diurnal fluctuations, we simulated 10,000 daily treatment differences for both soil temperature and moisture using a Monte Carlo approach. These differences are plotted as daily means with associated 95% confidence intervals (CI) and were analyzed alongside daily air temperature and precipitation data to evaluate warming–induced drying effects in the IR–heated plots. Daily precipitation data were inspected before plotting to remove missing values (i.e., negative values recorded as -99), producing a total of 1775 hourly observations after cleaning from January 2023 to July 2024. Monthly atmospheric and soil abiotic conditions are also reported using the same approach.

We used mixed–effect models as primary statistical framework to assess treatment effects on abiotic variables and soil GHG fluxes, incorporating random temporal and spatial effects to account for repeated measures, temporal (i.e., sampling day), and topographic variation (i.e., plot). For soil GHG fluxes, collar ID and installation date were included as an additional random effect to control for potential biases associated with finer spatial scales and collar deployment (Ma et al., 2023). We used Linear Mixed-Models (LMMs) to test for treatment effects on soil abiotic and GHG flux variables, with degrees of freedom and *p*-values estimated using Satterthwaite's approximation. When the normality assumption of LMM residuals was violated, we employed Generalized Additive Mixed Models (GAMMs) with a Gaussian response, accounting for the same temporal, spatial, and collar artifact random effects using penalized regression splines. Smoothing parameters were estimated using Restricted Maximum Likelihood (REML) method, which evaluates the residual variation after accounting for fixed effects to provide unbiased estimates of random effect variances and improve the accuracy of model residuals. Model fits between LMMs and GAMMs were additionally evaluated using Akaike Information Criterion (AIC) and Bayesian Information Criterion (BIC).

Analysis on soil GHG fluxes were performed using discrete flux measurements collected during both field campaigns. To evaluate the robustness of treatment effects to flux calculation methods and quality control (QC) decisions, we conducted a sensitivity analysis comparing linear and exponential chamber flux fits across a range of R^2 threshold cutoffs (0.70, 0.80, 0.85, 0.90, 0.92, and 0.95; Figs. SM2.1–SM2.3; Tables SM2.1–SM2.3). Distributions of R^2 values for both linear and exponential fits of soil CO_2 and CH_4 fluxes were skewed, with median values exceeding 0.97 across treatments (Fig. SM2.1; Table SM2.1). Control plots generally exhibited greater variability and a higher number of outliers than Warming plots for both gases and fitting approaches, resulting in a larger fraction of observations removed under increasingly stringent R^2 thresholds (Fig. SM2.2; Table SM2.2). Treatment effects on soil CO_2 and CH_4 fluxes were consistent across all R^2 thresholds and did not differ between linear and exponential fitting approaches (Table SM2.3 and Table SM2.4). However, linear flux estimates yielded lower AIC values than exponential estimates across thresholds (Table SM2.3 and SM2.4), indicating a statistically better fit at the mixed–model level. Despite this, we conservatively opted to use exponential flux estimates at an optimal QC threshold ($R^2 = 0.95$ for soil CO_2 efflux and $R^2 = 0.85$ for soil CH_4 efflux) for several reasons. First, exponential models better represent gas diffusion gradients and account for non–linear concentration changes during chamber closure (Forbrich et al., 2010; Silva et al., 2015). Indeed, diagnostic comparisons revealed that linear fits tend to underestimate high positive CO_2 and CH_4 fluxes and overestimate negative CH_4 fluxes (uptake) relative to exponential fits (Fig. SM2.3). Second, the selected R^2 thresholds minimized AIC values among exponential models while limiting data loss to moderate QC levels in both LMMs and GAMMs (approximately 2–10% of observations removed for soil CO_2 efflux and 4–28% for soil CH_4 efflux, depending on treatment and campaign; Fig. SM2.2; Tables SM2.2–SM2.4). Together, these results demonstrate that treatment effects are robust to flux calculation and QC choices, and that the selected approach provides a conservative and physically grounded basis for inference. The total number of observations per treatment used in all further analyses are 238 for soil CO_2 and 204 for soil CH_4 effluxes including all campaigns.

Next, we examined overall differences in soil GHG fluxes using violin plots stratified by treatment (Warming vs. Control), as well as by treatment and plot, including measurements for both summer campaigns (2023 and 2024). For soil CH_4 efflux measurements, any discrete negative flux value, including those near 0, is treated as a net soil CH_4 sink signal, while any positive value is considered a net CH_4 flux from soil to atmosphere (i.e., net CH_4 emission). The percentage of negative soil CH_4 fluxes, together with their 95% binomial confidence interval (CI), was used to estimate net soil CH_4 sink efficiency between treatment and within plots. We then assessed temporal patterns in treatment effects on soil CO_2 and CH_4 fluxes by analyzing measurements averaged by treatment and plots across sampling days. Mixed–effect models were also fitted to test the effect of treatments on soil CO_2 and CH_4 effluxes including their interaction with summer campaigns. This approach was used to explicitly evaluate whether treatment effects varied across summer campaigns while controlling for temporal and spatial structure, repeated measurements, and collar deployment biases. Furthermore, treatment effects were evaluated separately for each summer campaign to provide additional insight into potential temporal variability in treatment responses.

We examined whether variation in soil abiotic variables explained differences in soil GHG fluxes between treatments. To ensure temporal consistency, soil abiotic variables were matched to soil GHG flux measurements collected during the same measurement hours and dates, using the mean of sensor readings recorded at the start time of each chamber closure for each plot. First, we evaluated whether variation across soil GHG flux values between treatments corresponded to shifts in $\Delta T_{Warming\text{-}Control}$ and $\Delta VWC_{Warming\text{-}Control}$. Then, we modeled soil CH_4 and CO_2 effluxes measured at discrete times as functions of soil temperature and moisture. Because greenhouse gas emissions may respond linearly (Wan et al., 2007) or nonlinearly (e.g., 2^{nd} order quadratic) (Carey et al., 2016; Zhao et al., 2019) to abiotic conditions, we applied both model types. Model selection was based on BIC and AIC values. For soil CO_2 fluxes, an additional quadratic model was applied to ln–transformed efflux values following Carey et al. (2016) and compared with other model fits. After selecting the best–fitting models, we compared coefficients between treatments to assess differences in mechanistic responses to soil temperature and moisture, following the approach of Carey et al. (2016). Finally, we evaluated the response of soil CH_4 fluxes to soil CO_2 effluxes to assess whether net CH_4 uptake correlates positively or negatively to soil respiration in both treatments.

All maps, data cleaning, and statistical analyses were conducted in RStudio (Posit team, 2025) using the following R packages: *tidyverse* (Wickham et al., 2019), *ggpubr* (Kassambara, 2023), *viridisLite* (Garnier et al., 2023), *lubridate* (Grolemund and Wickham, 2011), *car* (Fox and Weisberg, 2019), *readxl* (Wickham and Bryan, 2025), *lmerTest (Kuznetsova et al., 2017), mgcv* (Pedersen et al., 2019), *scales* (Wickham et al., 2023), *writexl* (Ooms, 2025), *broom.mixed* (Bolker and Robinson, 2024), *tigris* (Walker, 2025), *ggspatial* (Dunnington, 2023), *terra* (Hijmans, 2025a), *elevatr* (Hollister et al., 2023), *tidyterra* (Hernangómez, 2023), *sf* (Pebesma, 2018), *raster* (Hijmans, 2025b), *purrr* (Wickham and Henry, 2025), and *gridExtra* (Auguie and Antonov, 2017).

3. Results

3.1. Soil and atmospheric abiotic variables

For the study period (January 2023 to July 2024), the realized experimental warming treatment within 0–10 cm depth resulted in a significant net increase in soil temperature of 1.95°C (LMM 95% CI = 1.10–2.80°C; $p < 0.001$; Table 1), while 0–10 cm depth soil moisture in warming plots was fairly similar to that in control plots (i.e., ~1% lower; LMM 95% CI = -5.46–3.48°C; $p = 0.57$; Table 1; Fig. 2, Fig. SM1.1, Table SM1). Residual diagnostic indicated no violation of the normality assumption for LMMs in both soil temperature and moisture measured within 0–10 cm soil depth (Fig. SM1.3). Spatial heterogeneity had a minor contribution to treatment differences, as indicated by the lower variance and 1σ values for plot–level random effects compared to the residuals (Table 1; Fig. SM1.2). In contrast, temporal variability played a major role in shaping differences in soil abiotic conditions as shown in Fig. 2a-b and Table 1 (see also Fig. SM1.1 and Table SM1).

Daily and monthly variation in soil temperature and moisture within 10 cm depth fluctuated between treatments, reflecting seasonal and short–term changes in atmospheric environmental drivers (Fig. 2; Fig. SM1.1; Table SM1). As shown in Fig. 2c, warmer and drier soil conditions were especially pronounced during the dry winter months (January to March), when air temperature and precipitation were lower compared to other months of 2023 and 2024 (i.e., around 22°C and lower than 30 mm/day, respectively). For example, in March 2023, soil temperature in the warmed plots was on average 3.57 °C higher, and soil moisture was 4.78% lower than in control plots (Fig. 2; Fig. SM1.1; Table SM1). Similar patterns were observed in March 2024, with differences of 2.37 °C and 0.37 % for soil temperature and soil moisture, respectively (Fig. 2, Fig. SM1.1, and Table SM1). As air temperature and precipitation increased toward the wet season in both years, mean air temperatures rose to ~27 °C, while precipitation was more variable, ranging from 7 mm/month (July 2024) to 465.5 mm/month (April 2023; Fig. 2, Fig. SM1.1, Table SM1). These patterns were especially evident during the soil gas efflux campaigns (June–August 2023 and June–July 2024), when treatment differences in soil temperature and moisture became more variable and at times approached zero (Fig. 2, Fig. SM1.1, Table SM1).

3.2. Soil greenhouse gases measurements

3.2.1. Soil CO_2 efflux

Soil CO_2 effluxes in the Control and Warming treatment plots averaged 2.33 ± 0.10 (mean ± 1σ; $n = 119$) and 3.62 ± 1.33 μmol m^{-2} s^{-1} (mean ± 1σ; $n = 119$), respectively, when combining measurements from the June–August 2023 and June–July 2024 campaigns (Table 2). Overall, the density distributions of soil CO_2 effluxes aggregated by summer campaigns shown in Fig. 3a were skewed for both treatments, with Control plots displaying a multimodal distribution.

Comparison between LMMs and GAMMs indicated that GAMMs better captured treatment effects and the observed distributional shapes. Specifically, LMM residuals violated the normality assumption (Fig. SM3.1a), whereas GAMMs yielded lower information criteria values ($AIC_{LMM} = 714.40$, $AIC_{GAMM} = 692.98$; $BIC_{LMM} = 738.71$, $BIC_{GAMM} = 732.84$; Table SM3.1). The Warming treatment on soil CO_2 effluxes including for both summer campaigns was significantly higher by 1.30 μmol m^{-2} s^{-1} (GAMM 95% CI = 0.14, 2.46 μmol m^{-2} s^{-1}; Table 3a), which corresponded to a significant, net 56.44% increase in soil respiration (95% CI = 6.25, 106.23%; Table 3a).

Among random effects, variation among plots significantly influenced soil CO_2 efflux distributions across both treatments when combining summer campaigns ($F = 37.90$, $p < 0.001$; Table 3a). In contrast, no significant contribution to treatment differences was detected for day collar installation date ($p > 0.05$; Table 3a). Similarly, there are no random effects on treatment differences by collar ID ($F \sim 0$; $p > 0.05$; Table 3a). Indeed, soil CO_2 effluxes measured from collars within the same plots yielded similar central tendency values across both summer campaigns (Fig. SM3.2a–b and Table SM3.2). As illustrated in Fig. 3b and Table 2, soil CO_2 effluxes aggregated across both summer campaigns exhibited similar mean and median values among Warming plots, although plots 2 and 4 showed the greatest variability in flux measurements. Conversely, Control plots displayed variable degrees of skewness and differences in central tendency, with plot 1 exhibiting the highest mean and median values and plot 5 the lowest across the June–August 2023 and June–July 2024 campaigns (Fig. 3b; Table 2).

3.2.2. Soil CH_4 efflux

During the summer campaigns June–August 2023 and June–July 2024 campaigns at the TRACE site, mean soil CH_4 fluxes in Control and Warming plots were -0.31 ± 0.49 (mean ± 1σ; $n = 88$) and -0.41 ± 0.36 ηmol m^{-2} s^{-1} (mean ± 1σ; $n = 116$), respectively (Table 2; Fig. 3c). Similarly to soil CO_2 flux measurements, soil CH_4 effluxes in both treatments had skewed distributions when including values for all summer campaigns, with fluxes in Control treatment showing a bimodal distribution as displayed in Fig. 3c. Negative soil CH_4 effluxes, indicative of net soil CH_4 uptake, differed in proportion between treatments, accounting for 87.50 % (95% CI = 78.99, 92.87%) of observations in

Table 2
Summary statistics of soil CO_2 and CH_4 effluxes measured during 2023 and 2024 field campaigns under Control and Warming treatments. The table reports summary statistics grouped by treatment, and by treatment and plots. Each grouping reports treatment type, plot (if applicable), number of measurements (n), and central tendency values for each soil greenhouse gas (mean ± 1σ and median). For soil CH_4 effluxes, net uptake proportion (%), defined as the percent value of n flux values <0 relative to total n (Uptake %, (Mean, 95% CI)) is reported to emphasize CH_4 sink behaviors across treatments and plots.

Summary by Treatment (Summer campaigns June-August 2023 and June-July 2024)

Treatment	Soil CO_2 efflux			Soil CH_4 efflux			
	n	**Mean ± 1σ**	**Median**	***n***	**Mean ± 1σ**	**Median**	**Uptake % (Mean, 95% CI)**
Control	119	2.33 ± 0.10	2.28	88	-0.31 ± 0.49	-0.24	87.50 [78.99, 92.87]
Warming	119	3.62 ± 1.33	3.22	116	-0.41 ± 0.36	-0.41	98.28 [93.93, 99.53]

Summary by Treatment and Plot (Summer campaigns June-August 2023 and June-July 2024)

Treatment	Plot	Soil CO_2 efflux			Soil CH_4 efflux			
		n	**Mean ± 1σ**	**Median**	***n***	**Mean ± 1σ**	**Median**	**Uptake % (Mean, 95% CI)**
Control	1	42	3.10 ± 0.63	3.07	40	-0.62 ± 0.42	-0.68	97.50 [87.12, 99.56]
Control	3	39	2.25 ± 0.64	2.09	33	-0.14 ± 0.16	-0.14	93.94 [80.39, 98.32]
Control	5	38	1.58 ± 1.03	1.20	15	0.17 ± 0.58	0.06	46.67 [24.81, 69.88]
Warming	2	41	3.97 ± 1.40	3.82	39	-0.48 ± 0.23	-0.52	100.00 [91.03, 100]
Warming	4	40	4.02 ± 1.45	3.46	40	-0.53 ± 0.26	-0.46	100.00 [91.24, 100]
Warming	6	38	2.83 ± 0.57	2.67	37	-0.22 ± 0.47	-0.27	94.59 [82.30, 95.50]

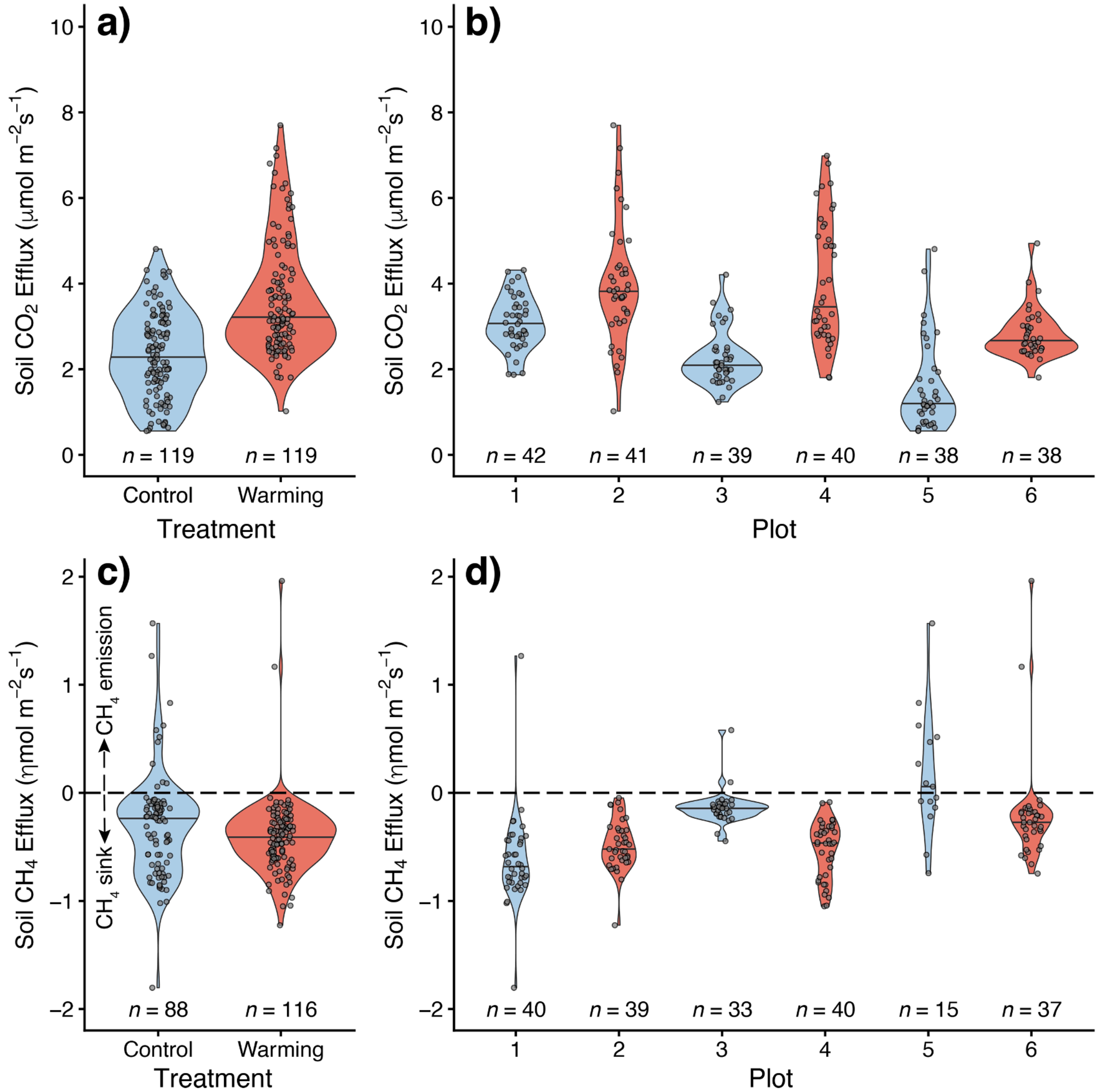

Fig. 3. Warming had a statistically significant effect on soil respiration, but not for soil CH_4 effluxes, where variation was largely driven by between-plot differences. Panels **a)** and **b)** show violin plots of soil CO_2 efflux grouped by treatments (panel **a**) and by treatment and plot (panel **b**). Panels **c)** and **d)** show violin plots of soil CH_4 effluxes grouped similarly to panels **a)** and **b)**, respectively. Horizontal solid lines indicate median values, while grey points are discrete soil greenhouse gas (GHG) measurements used to build the violins. Distributions are color-coded by treatment: light blue for Control and red for Warming. The dashed line at 0 ηmol m^{-2} s^{-1} in panels **c)** and **d)** marks the transition from negative to positive CH_4 fluxes, distinguishing between methane uptake (sink) and emission (source). Each distribution reports the sample size (*n*) used to generate the violin shapes.

Control and 98.28 % (95% CI = 93.93, 99.53%) in Warming plots across both summer campaigns (Fig. 3c and Table 2).

Model selection criteria for mixed–effect models of treatment effects on soil CH_4 effluxes across both summer campaigns yielded contrasting results, with BIC values favoring LMM model over the GAMM one (BIC_{LMM} = 193.43, BIC_{GAMM} = 222.64; Table SM3.1), whereas AIC supported GAMM as the better–fitting model (AIC_{LMM} = 170.21, AIC_{GAMM} = 135.31; Table SM3.1). This discrepancy likely reflects differences in model complexity, as GAMMs used a higher effective number of degrees of freedom (df_{LMM} = 7, df_{GAMM} = 26.32; Table SM3.1) and are therefore more strongly penalized by BIC. Additionally, the LMM residuals violated normality assumptions (Fig. SM3.1). Consequently, GAMMs were retained as a parsimonious framework to test treatment effects on soil CH_4 effluxes while accounting for temporal, spatial, and collar artifact–related random effects.

The GAMM estimated a -0.22 ηmol m^{-2} s^{-1} contrast between in soil CH_4 fluxes under Warming treatment relative to Control plots across both summer campaigns (95% CI = -0.73, 0.29 ηmol m^{-2} s^{-1}, Table 3b). This corresponded to an estimated 114.09% change relative to Control treatment (95% CI, -150.07, 378.24%, Table 3b), although the warming effect was not statistically significant (p = 0.40; Table 3b). When accounting for spatial random effects, variability in CH_4 fluxes was driven primarily by plots (F = 42.28; $p < 0.001$; Table 3b) rather than among collars (F = 0.53; p = 0.18; Table 3b, Fig. SM3.2, Table SM3.2). As illustrated in Fig. 3d and Table 2, no positive CH_4 fluxes were observed in the warmed plots 2 and 4 during both summer campaigns, which displayed similar skewed distributions and central tendency values. In contrast, the IR–warmed plot 6 showed slightly higher fluxes (Fig. 3d and Table 2), with a small number of positive efflux outliers reducing net soil CH_4 uptake from 100% to on average 94.59% (95% CI = 82.30, 95.50%; Fig. 3c–d; Table 2). Control plots exhibited different skewed shapes, with central tendency increasing and net CH_4 uptake decreasing from plot 1 to 5 (Fig. 3d and Table 2). In addition to spatial effects, sampling day (date) explained significant variation in soil CH_4 dynamics across both summer campaigns independent of treatment effects (F = 3.00; $p < 0.001$; Table 3b). No unexplained variation attributed to collar

Table 3
Generalized additive mixed-effects models (GAMMs) for soil CO_2 and CH_4 efflux measured in June–August 2023 and June–July 2024. Separate models were fitted for soil respiration (a) and soil CH_4 efflux (b), with Treatment (Warming vs. Control) as a fixed effect. Temporal, spatial, and collar artifacts dependencies were accounted for by including day, plot, collar ID, and collar installation age as random effects. Fixed effect estimates are reported with their standard error (SE), t-values (*t*), and *p*-values (*p*). Random effects report the estimated degrees of freedom (Estimated df), reference degrees of freedom (Reference df), F-values (F), and *p*-values (*p*) of variability in baseline intercept values across groups not explained by fixed effects. The Estimated df reflects how much the random intercepts are allowed to vary across groups, whereas the Reference df is the nominal number of degrees of freedom used to test significance of the random effects. The F- and *p*-values test whether the random intercepts explain significant variability in baseline fluxes not captured by fixed effects. The asterisks denote levels of statistical significance: $p < 0.05$ (*), $p < 0.01$ (**), and $p < 0.001$ (***).

GAMM: Soil Flux ~ Treatment + s(Time(Day)) + s(Plot) + s(Collar ID) + s(Collar age)

a) Soil CO_2 Efflux				
Fixed effects	**Parameter**	**SE**	***t***	***p***
Control	2.31	0.42	5.52	9.06E-08***
Warming *vs.* Control	1.30	0.59	2.20	0.03*
Random effects	**Estimated df**	**Reference df**	**F**	***p***
s(Date)	3.09E-03	20	1.52E-04	0.48
s(Plot)	3.54	4	37.90	1.74E-06***
s(Collar installation date)	3.77E-05	1	1.83E-06	0.83
s(Collar ID)	3.68	10	1.37	0.19
b) Soil CH_4 Efflux				
Fixed effects	**Parameter**	**SE**	***t***	***p***
Control	-0.19	0.19	-1.03	0.31
Warming *vs.* Control	-0.22	0.26	-0.85	0.40
Random effects	**Estimated df**	**Reference df**	**F**	***p***
s(Date)	14.25	20	3.00	2.40E-06***
s(Plot)	3.80	4	42.28	< 2.16E-16***
s(Collar installation date)	6.25E-05	1	2.20E-06	0.85
s(Collar ID)	2.22	10	0.53	0.18

installation dates was detected (i.e., 2016 and 2022; F ~ 0; $p = 0.18$; Table 3).

3.3. Soil greenhouse gases response to soil temperature and moisture

The GAMMs for soil CO_2 and CH_4 effluxes, including summer campaigns as a fixed effect and its interaction with Treatment, revealed that such interactions were statistically significant only for soil respiration ($p < 0.001$; Table SM3.3a), while soil CH_4 efflux variation was driven by temporal variability across days irrespective of treatment differences ($p < 0.001$; Table SM3.3b, see also Table 3b). Temporal patterns of soil CO_2 and CH_4 fluxes displayed in Fig. 4a-b and Table 3, averaged by treatments and dates, showed either directional shifts in soil GHG flux values between treatments or substantial variation across sampling days irrespective of warming effects (see also Tables SM3.3, SM3.4, SM4). The GAMM restricted to the 2023 summer campaign produced results consistent with the full models (Table 3) that included data from all summer campaigns; this resulted in 68.82 % (95% CI = 7.49, 130.15%) shift in soil CO_2 effluxes and a -203.57 % (95% CI = -684.59, 245.45%) change in soil CH_4 efflux values under Warming treatment, but directional shifts due to warming were statistically significant only for soil respiration ($p < 0.05$ and $p > 0.05$, respectively; Tables 3, SM3.3, SM3.4). However, treatment differences were not significant during June–July 2024 ($p > 0.05$; Table SM3.5), indicating that measurements taken during the 2023 summer campaign primarily drive the observed treatment effects on soil respiration when integrating flux values from both summer campaigns (Table 3). As seen in Fig. 4b, soil CH_4 values averaged by treatment and dates in the Warming plots often run parallel to, and closely follow, those of the Control plots; yet notable and variable negative offsets in the Warming treatment are evident between July 7 and July 24, 2023 (see also Table SM4). The GAMMs models for individual years indicate no substantial treatment effect on soil CH_4 effluxes, but variation was sensitive to plot and days (Table SM3.4b and SM3.5b). This variability across sampling days in fluxes and the offset between treatments, when present (Fig. 4a-b; Table SM4), mirrored temporal variation in soil moisture and temperature differences within 10 cm between treatments calculated during the same temporal window and dates of soil GHG fluxes as shown in Fig. 4c–d (see also Table SM4). Together, this suggests a potential control of soil moisture and temperature on soil GHG fluxes in both treatments.

Fig. 5 shows that the relationships between soil GHG fluxes and abiotic variables within 0–10 cm depth, aggregated by sensor location within each plot and matched by soil GHG measurement hour, differ by gas type and treatment. Responses of soil GHG measurements to soil abiotic variables were evaluated using models fitted without random effects (Fig. 5, Supplementary Materials SM5). Among linear and quadratic models tested to describe the response of soil respiration to abiotic variables, the quadratic model using ln–transformed CO_2 fluxes and soil moisture (VWC, volumetric water content) performed best (AIC = 82.68 and BIC = 102.02 for ln (CO_2 efflux) ~ $\beta_0 \times \beta_1$ VWC + $\beta_2 \times$ VWC^2 × Treatment; Fig. 5a, Table 4a, and Table SM5). Similarly, the quadratic model using ln–transformed CO_2 fluxes and soil temperature outperformed other linear and quadratic alternatives (AIC = 79.63 and BIC = 99.26 for ln (CO_2 efflux) ~ $\beta_0 \times \beta_1$ Temperature + β2 × Temperature^2 × Treatment; Fig. 5b, Table 4b, and Table SM5.2).

Ln–transformed soil CO_2 effluxes shown in Fig. 5a exhibited a significant, negative quadratic relationship with volumetric water content (VWC) in both treatments, though the model explained little variance under both Control ($R^2 = 0.13$, $p < 0.05$; Table 4a) and Warming treatment ($R^2 = 0.11$, $p < 0.05$; Table 4a). The Intercept coefficients (β_0) in the warmed plots were significantly higher than those in the Control treatment ($p < 0.001$; Fig. 5a, Table 4a, Table SM5.1), whereas the linear and quadratic terms (β_1 and β_2) did not significantly vary ($p > 0.05$; Fig. 5a, Table 4a, Table SM5.1).

By contrast, ln–transformed CO_2 fluxes showed a weak, positive, quadratic response to temperature in the Control treatment ($R^2 = 0.20$, $p = 0.001$), while the relationship under Warming was significantly weaker, negative, and non-significant ($R^2 = 0.08$, $p = 0.08$; Fig. 5b). As illustrated in Fig. 5b and Table 4b, the intercept (β_0) in Warming plots was lower but not statistically different from that in the Control treatment ($p > 0.05$), while both linear and quadratic slopes (β_1 and β_2) were significantly lower in Warming relative to Control treatment ($p < 0.01$ and $p < 0.05$, respectively; see also Table SM5.2).

In contrast to CO_2 fluxes, linear models shown in Fig. 5c-d best described the response of soil CH_4 efflux to abiotic conditions. The linear model using soil moisture (VWC) outperformed the quadratic version (AIC = 92.66 and BIC = 106.02 for CH_4 efflux ~ $\beta_0 \times \beta_1$ VWC × Treatment; Table SM5.3), and the same held for soil temperature (AIC = 118.20 and BIC = 131.79 for CH_4 efflux ~ $\beta_0 \times \beta_1$ Temperature × Treatment; Table SM5.4). For soil moisture, both Control and Warming treatments had a weak, significant positive relationship with soil CH_4 effluxes as illustrated in Fig. 5c and Table 4c ($R^2 = 0.27$ and $p < 0.001$ in Control treatment, and $R^2 = 0.28$ and $p < 0.001$ in Warming treatment). The regression lines were nearly parallel, with intercepts (β_0) that differed significantly between treatments ($p < 0.001$; Table SM5.3), but not slope coefficients (β_1; $p > 0.05$; Table SM5.3).

While soil CH_4 effluxes responded similarly to varying soil moisture levels between Control and warmed plots, soil CH_4 dynamics showed different sensitivities to soil temperature between treatments. As shown in Fig. 5d and Table 4d, CH_4 effluxes in Control plots declined with increasing soil temperature, yielding weak, significant negative correlation ($R^2 = 0.18$, $p < 0.01$; see also Table SM5.4). However, in Warming

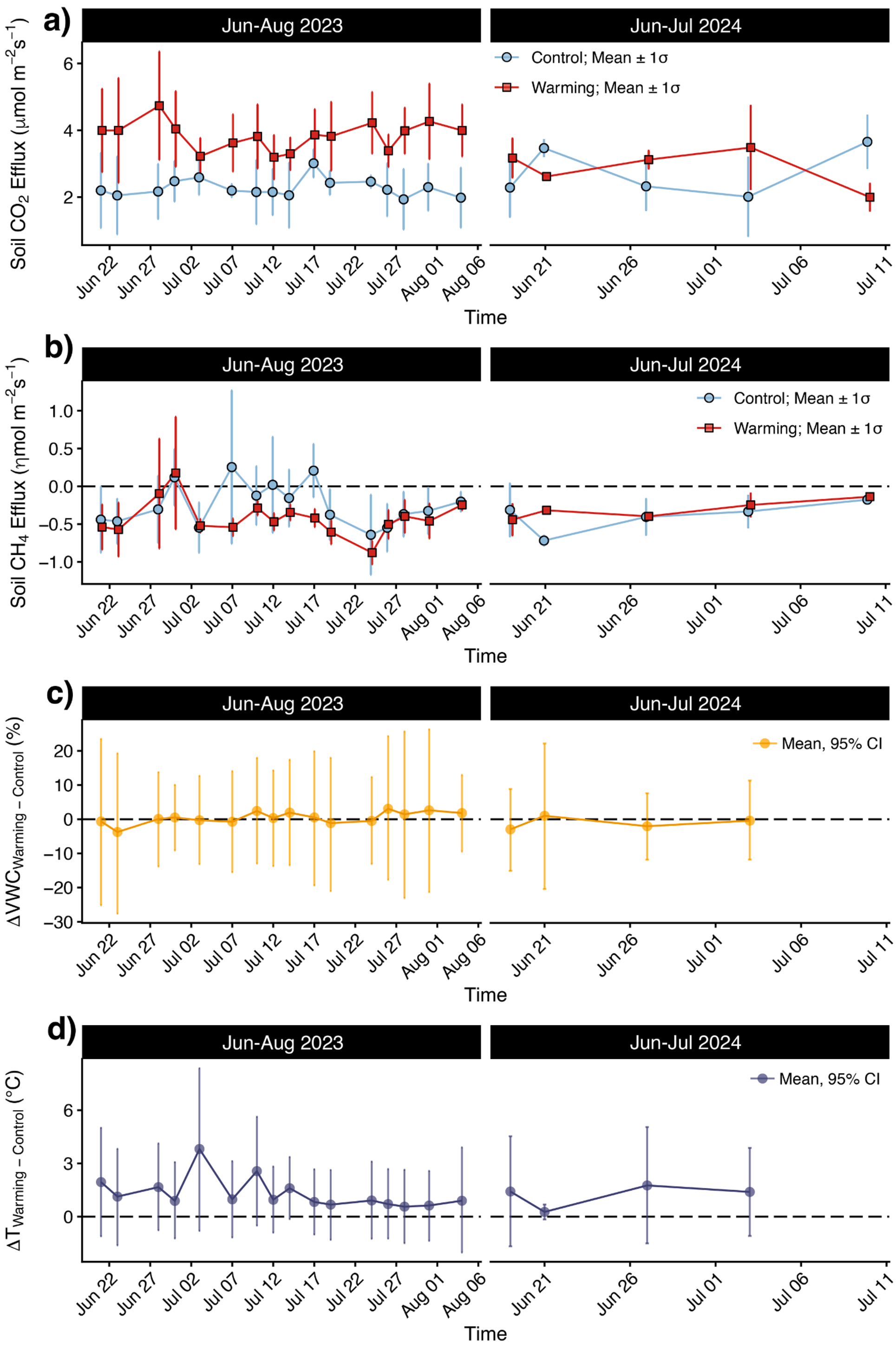

Fig. 4. Soil CO_2 and CH_4 effluxes varied in response to altered abiotic conditions, including increased temperature and reduced moisture under the Warming treatment. **a)** Time series of soil CO_2 effluxes averaged by treatment and date (total $n_{Control} = 60$, and $n_{Warming} = 57$) across measurement days for summer campaigns Jun–Aug 2023 and Jun–July 2024. **b)** Time series of net soil CH_4 effluxes (total $n_{Control} = 60$, total $n_{Warming} = 62$) averaged by treatment and date across measurement days for summer campaigns Jun–Aug 2023 and Jun–July 2024. The dashed black line marks the transition from negative to positive CH_4 fluxes; **c)** Differences in volumetric water content (i.e., soil moisture; yellow circles) between Warming and Control plots ($\Delta VWC_{Warming\text{-}Control}$; total $n_{Control} = 51$, total $n_{Warming} = 56$). **d)** Differences in soil temperature (violet circles) between Warming and Control plots ($\Delta T_{Warming\text{-}Control}$; total $n_{Control} = 51$, total $n_{Warming} = 61$). Soil moisture and temperature measurements used to calculate differences were collected at 0–10 cm depth, aggregated by sensor location within each plot, and matched to the temporal window of soil greenhouse gas (GHG) measurements (9:00 am–12:30 pm) on the same days, and averaged by date. Error bars represent one standard deviation (±1σ) in panels **a)** and **b)**, and 95% confidence intervals (CI) in panels **c)** and **d)**. Soil GHG values are color- and shape-coded by treatments in panels **a)** and **b)**: light blue circles for Control and red squares for Warming treatment. The horizontal dashed line at 0% and 0°C in panels **c)** and **d)** separates positive from negative differences in soil moisture and temperature, respectively.

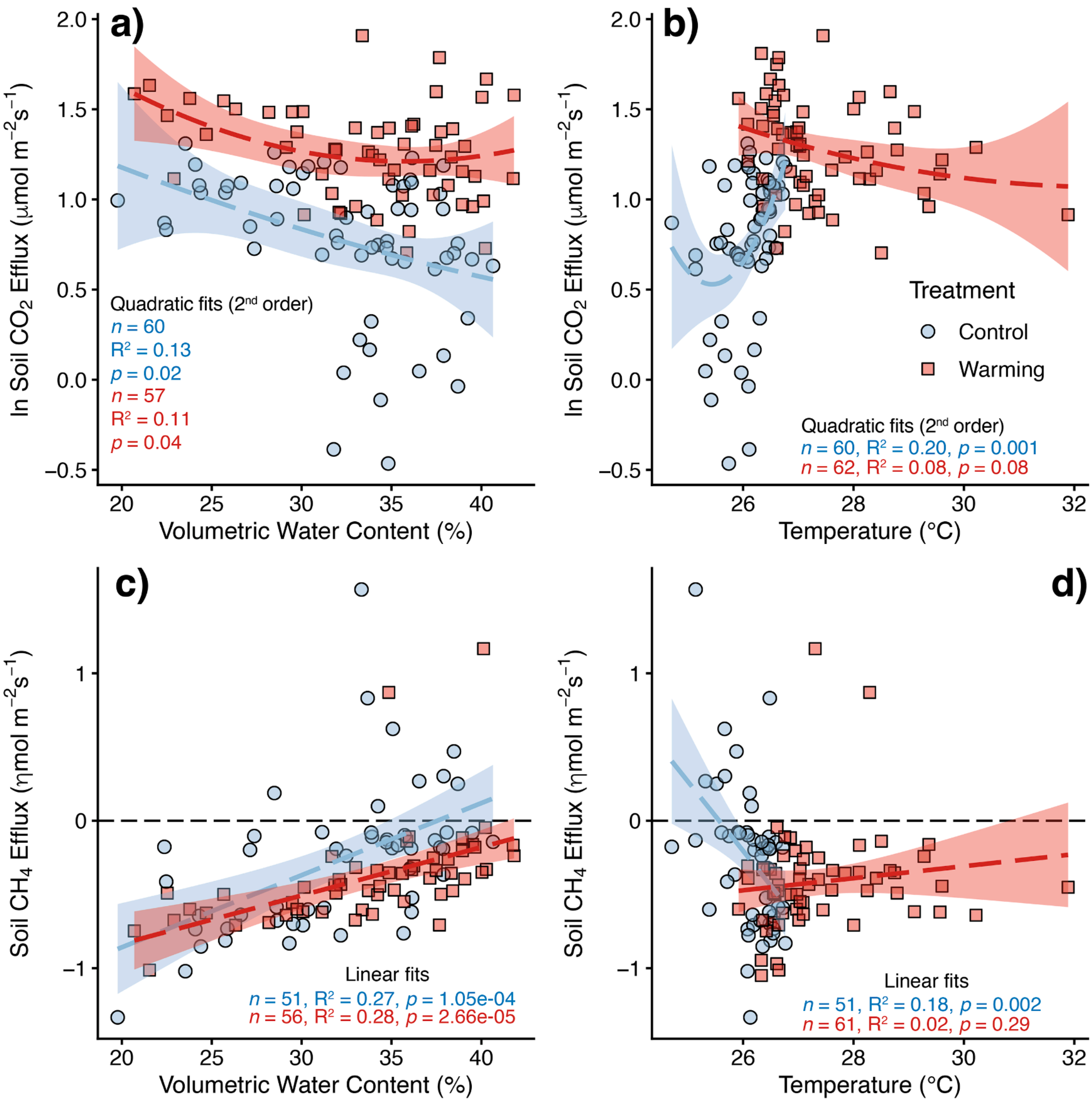

Fig. 5. Soil CO_2 and CH_4 effluxes often exhibited distinct responses to soil moisture and temperature under Control and Warming treatments. Panels **a)** and **b)** depict the quadratic response of discrete, ln-transformed CO_2 efflux to soil moisture and temperature, respectively. Panels **c)** and **d)** show the linear response of discrete soil CH_4 efflux to soil moisture and temperature, respectively. The black dashed line in panels **c)** and **d)** marks the transition from negative to positive CH_4 fluxes, distinguishing between methane uptake (sink) and emission (source). Soil moisture and temperature measurements were collected at 0–10 cm depth, aggregated by sensor location within each plot, and matched to the same measurement hours as the soil greenhouse gas (GHG) fluxes. Data points are shape- and color-coded: light blue circles for Control and red squares for Warming treatment. Model fits are shown as dashed lines with shaded areas representing standard error. The sample size (n), coefficient of determination (R^2), and p-value (p) describing the relationships between soil GHG effluxes and soil abiotic variables for each treatment are reported.

treatment, CH_4 effluxes showed no significant relationship with soil temperature ($R^2 = 0.02$, $p = 0.29$; Fig. 5d, Table 4d, and Table SM5.4). In this case, intercepts and slopes differed significantly between treatments ($p < 0.001$; Fig. 5d, Table 4d, and Table SM5.4).

3.4. Soil CH_4 relationship with soil respiration in control and warming treatments

Fig. 6 and Table 5 shows that soil CH_4 fluxes were negatively correlated with soil respiration rates in both treatments ($R^2 = 0.25$ and 0.28; $p < 0.001$ for Control and Warming treatments, respectively). While showing similar overall trends, both intercept and slope coefficients differed in magnitude between the two treatments (Fig. 6 and Table 5). An interaction model confirmed that the slope coefficients (β_1) differed significantly between treatments ($p < 0.05$; Table SM6), whereas the intercept (β_0) difference was not statistically significant ($p <$ 0.001; Table SM6).

4. Discussion

4.1. Weak warming manipulation effects still shaped soil GHG responses

Infrared–heated plots were consistently warmer and marginally drier than controls (Fig. 2, Fig. SM1.1, Table 1, Table SM1.1), with the magnitude of soil warming (~1.95°C) substantially lower than the surface warming experimental target (4°C; Kimball et al., 2018), consistent with expected attenuation down the soil profile. Soil moisture was more variable in the warmed plots than in the Control treatment, with values reaching volumetric water content (VWC) as low as ~17% in the Warming treatment in March 2023 (Fig. SM1.1b, Table SM1.1). However, mean soil moisture across both 2023 and 2024 campaigns did not differ significantly between treatments across the study period

Table 4
Model coefficients describing soil greenhouse gas responses to volumetric water content (VWC) and temperature within 10 cm depth under Control and Warming treatments. **a)** and **b)** report intercepts (β_0), linear slopes (β_1), and quadratic terms (β_2), with their standard error (SE), for the ln-transformed soil CO_2 efflux response to soil moisture and temperature, respectively. **c)** and **d)** show intercepts (β_0), linear slopes (β_1) with SE for the soil CH_4 efflux response to soil moisture and temperature, respectively. The table includes coefficient of determination (R^2) and *p*-value (*p*) of model fits. The asterisks denote levels of statistical significance: $p < 0.05$ (*), $p < 0.01$ (**), and $p < 0.001$ (***).

a) Parameters for ln (Soil CO_2 Efflux) ~ $\beta_0 + \beta_1 \times VWC + \beta_2 \times VWC^2$					
Treatment	**β_0 ± SE**	**β_1 ± SE**	**β_2 ± SE**	**R^2**	***p***
Control	0.77 ± 0.05	-1.14 ± 0.39	0.08 ± 0.39	0.13	0.02*
Warming	1.26 ± 0.03	-0.53 ± 0.25	0.40 ± 0.25	0.11	0.04*
b) Parameters for ln (Soil CO_2 Efflux) ~ $\beta_0 + \beta_1 \times T + \beta_2 \times T^2$					
Treatment	**β_0 ± SE**	**β_1 ± SE**	**β_2 ± SE**	**R^2**	***p***
Control	0.77 ± 0.49	1.24 ± 0.38	0.74 ± 0.38	0.20	0.001**
Warming	1.28 ± 0.03	-0.59 ± 0.27	-0.11 ± 0.27	0.08	0.08
c) Parameters for Soil CH_4 Efflux ~ $\beta_0 + \beta_1 \times VWC$					
Treatment	**β_0 ± SE**	**β_1 ± SE**	**R^2**	***p***	
Control	-1.84 ± 0.38	4.89 ± 1.16	0.27	1.05E-04***	
Warming	-1.49 ± 0.24	3.28 ± 0.71	0.28	2.66E-05***	
d) Parameters for Soil CH_4 Efflux ~ $\beta_0 + \beta_1 \times T$					
Treatment	**β_0 ± SE**	**β_1 ± SE**	**R^2**	***p***	
Control	12.03 ± 3.69	-0.47 ± 0.14	0.18	0.002**	
Warming	-1.53 ± 1.05	0.04 ± 0.04	0.02	0.29	

(Fig. 2b, Fig. SM1.1b, Table 1b, Table SM1.1). The fact that the warming effect on manipulated plots did not result in the expected warmer and drier soil conditions is best explained by several potential mechanisms: (*i*) the accumulation of surface litterfall intercepted radiative heat before it could reach the soil, buffering the warming effect (Reed et al., 2020); (*ii*) warming manipulation system malfunctioning, noticeable during periods of negligible differences in soil temperature and moisture between treatments (i.e., Soil $\Delta T_{Warming\text{-}Control}$ and $\Delta VWC_{Warming\text{-}Control}$ close or equal to 0; Fig. 2a–b, Fig. 4c–d; Fig. SM1.1, Table SM1.1, Table SM4); (*iii*) intense rainfall events increased soil moisture, enhancing latent heat dissipation and thereby lowering soil temperature (Wan et al., 2007), and/or increasing the specific heat of soils due to elevated VWC. All such potential mechanisms highlight the challenge of achieving consistent warming in tropical open–air field systems.

The compensatory effect of multiple mechanisms constraining the realized warming were evaluated by modelling the soil thermal conductivity (λ; Supplementary Material SM1.2, Fig. SM1.4), which integrates soil physical properties and conductive heat fluxes (Campbell, 1985; Xiong et al., 2023). Given the marginal differences in soil moisture between treatments (Fig. 2a-b, Fig. 4c-d; Fig. SM1.1, Table SM1.1, Table SM4), we expected soil thermal properties in warmed plots to dissipate heat similarly to those in Control soils. Assuming a soil clay content of 44% and a bulk density value of 0.50 g cm^{-3} following a survey at TRACE conducted in the horizon A1 (2–18 cm depth) near experimental plots in 2019, we observed only subtle differences in thermal conductivity between treatments (i.e., $\Delta\lambda_{Warming\text{-}Control}$) ranging from ~-2 to ~1.5% during the study period (i.e., January 2023–July 2024; Fig. SM1.4b), including during soil GHG sampling campaigns (Supplementary Materials SM1.2). Together, these results indicate the combining, interactive effects of rainfall events, surface litter accumulation, and occasional infrared heating system limitations constrained effective heat transfer from IR–radiators to soils, resulting in similar soil thermal conductivity values between treatments and limiting the realization of the intended warming signal (i.e., warmer and drier soils relative to controls).

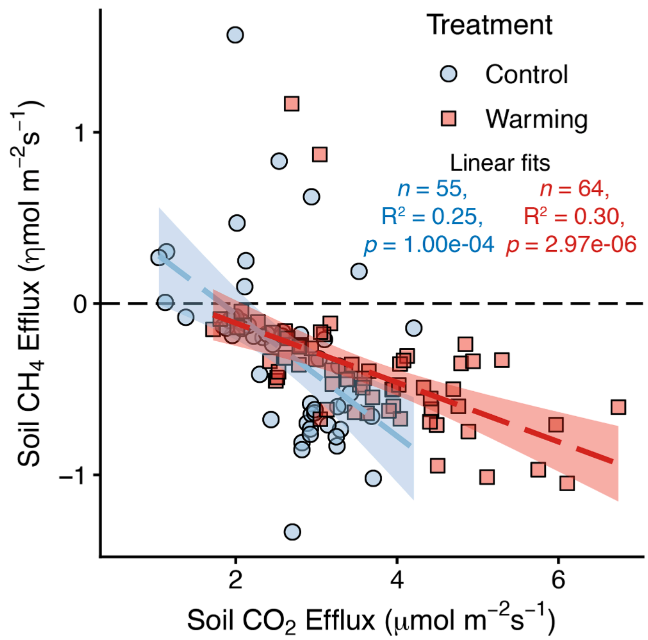

Fig. 6. Uptake of methane (sink) is enhanced with increasing respiration values in both Control (light blue circles) and Warming (red squares) treatments. Soil greenhouse gas (GHG) fluxes were aggregated by measurement hours and dates within each treatment. Dashed lines with shaded ribbons indicate the linear correlations and the standard errors between soil CH_4 and CO_2 effluxes, color-coded by treatment. Note the differences in intercepts and slopes between treatments. The black, horizontal, dashed line separates negative from positive CH_4 flux values, distinguishing between methane uptake (sink) and emission (source), respectively. The sample size (*n*), coefficient of determination (R^2), and *p*-value (*p*) describing the relationships between soil GHG effluxes for each treatment are reported.

Table 5
Linear model coefficients for soil CH_4 vs CO_2 efflux in Control and Warming treatments aggregated by measurement hours and dates. The table shows intercept (β_0), slope (β_1), coefficient of determination (R^2) and *p*-value (*p*). Intercepts and slope are reported with their standard error (SE). The asterisks denote levels of statistical significance: $p < 0.05$ (*), $p < 0.01$ (**), and $p < 0.001$ (***).

Parameters for Soil CH_4 Efflux ~ Soil CO_2 Efflux				
Treatment	**β_0 ± se**	**β_1 ± se**	**R^2**	***p***
Control	0.65 ± 0.23	-0.36 ± 0.08	0.25	1.00E-04***
Warming	0.23 ± 0.03	-0.03 ± 0.02	0.30	2.97E-06***

With respect to surface litterfall and potential artifacts associated with the IR heating system, warming effects were strongly modulated by precipitation regimes during the soil GHG measurement campaigns of 2023 and 2024 (Fig. 2, Fig. SM1.1, Table 1, Table SM1). During June–August 2023, persistent daily rainfall ranging from weak to heavy (up to ~50 mm day^{-1}) resulted in smaller differences in soil temperature and moisture between treatments (Fig. 2, Fig. SM1.1, Table 1, Table SM1.1). In contrast, precipitation approached 0 mm day^{-1} during the June–July 2024 campaign, leading to warmer and marginally drier soil conditions in the warming treatment relative to ambient plots (Fig. 2, Fig. SM1.1, Table 1, Table SM1.1). These shifts in soil temperature and moisture were sufficient to alter soil GHG fluxes between treatments during different field campaigns (Fig. 4, Fig. 5, Supplementary Materials SM4, SM5), underscoring the sensitivity of tropical soils to relatively small abiotic perturbations.

4.2. Warming manipulation experiment did not alter soil CH_4 uptake buffering capacity against soil CH_4 emissions

Contrary to expectations, the manipulation experiment did not produce consistent treatment differences in soil GHG fluxes across the summer campaigns (Fig. 3, Table 2, and Table 3). Instead, the warming response varied among gases and across years, indicating that treatment effects were modulated by interannual differences in hydroclimatic conditions. In particular, the contrasting precipitation regimes of summer field campaigns 2023 and 2024, characterized by wetter conditions during the summer months in 2023 and a pronounced drought during the summer field campaign 2024 (Fig. 2, Table SM1), likely mediated the effects of the realized soil warming, soil moisture, and potentially nutrient availability during post–hurricane recovery, modulating the response of soil GHG fluxes. Alternatively, the lack of treatment effect on soil CH_4 fluxes, and on soil respiration during the summer campaign 2024, could be an artifact effect due to long–term collar deployment.

Soil GHG fluxes at TRACE have declined over time (Wood et al., 2025; this study), suggesting that experimental artifacts, particularly the long–term use of the same collars, could be contributing to this trend. Such a decline could provide another alternative explanation for why treatment differences in soil respiration rates were low in 2024 and no effect of warming was observed on soil CH_4 fluxes (GAMMs $p > 0.05$; Fig. 3, Fig. 4, Table 2, Table 3, Table SM3.3, Table SM3.4, and Table SM3.5). Collar effects are known to result in an underestimate of soil GHG fluxes by severing roots and mycorrhizae and altering soil physicochemical properties, thereby affecting heterotrophic activity and soil gas exchange (Ma et al., 2023). Although collar installation date, modeled as a random effect, did not account for a significant proportion of variance in soil GHG fluxes (GAMMs $p > 0.05$; Table 3, Table SM3.3, Table SM3.4, and Table SM3.5), we acknowledge the possibility that collar artifacts have reduced the magnitude of soil GHG fluxes since collars were installed in 2016 and 2022. For example, Wood et al. (2025) reported mean diurnal soil respiration rates as high as ~20 and ~30 μmol m^{-2} s^{-1} for Control and Warming treatments, respectively, after one year (2016–2017) of experimental warming during the summer months at the TRACE site, values roughly an order of magnitude higher than those recorded during our 2023 and 2024 summer field campaigns (Fig. 3a–b, Fig. 4a). Net soil CH_4 fluxes may have undergone a similar decline, considering that soil methane flux dynamic is tied to soil respiration (Fig. 6, Table SM6), but the lack of continuous CH_4 measurements prevents us from quantifying this change over time. While collar artifacts may have reduced the absolute magnitude of fluxes in both treatments, they should not eliminate directional treatment effects if such effects are present. Indeed, the realized warming at TRACE significantly increased soil respiration rates by ~1.30 – ~1.55 μmol m^{-2} s^{-1} relative to control plots, at least during June–August 2023 (GAMMs $p = 0.03$; Fig. 3a–b, Fig. 4a, Table 2, Table 3a, Table SM3.4a), suggesting that the observed directional shifts most likely reflect genuine biogeochemical responses that have been attenuated by long–term collar effects. Thus, collar artifacts alone cannot explain the pronounced warming response in soil respiration observed during summer months in 2023, nor the lack of significant directional warming effects on net soil CH_4 uptake during the summer campaigns 2023 and 2024.

Warming could have improved aeration by slightly enhancing soil drying and raising temperatures. In Oxisols like those at TRACE (Beinroth et al., 2003; Muñoz et al., 2018), such changes are expected to increase oxygenation in surface layers where methanotrophs are most active (Nazaries et al., 2013; Wanyama et al., 2019; Zhao et al., 2019). Indeed, in control plots, drier and warmer conditions increased both soil respiration and CH_4 uptake (Fig. 5, Table 4, Supplementary Material 5). However, in warmed plots, soil GHG fluxes showed often a weaker dependence on abiotic drivers. Soil respiration, for example, became decoupled from measurement of moisture, and CO_2 fluxes mildly decrease above ~26.5°C ($p < 0.05$; Fig. 5a–b, Table 4, Table SM5.1–5.2). Similarly, net CH_4 uptake in warmed soils was higher than in controls but remained relatively stable across the upper temperature range ($p < 0.05$; Fig. 5d, Table 4, Table SM5.4). Importantly, soil CH_4 fluxes were also linearly related to soil moisture ($p < 0.001$; Fig. 5c, Table 4, Table SM5.3), consistent with prior studies showing that moisture is a dominant abiotic control of methane exchange (Nazaries et al., 2013; O'Connell et al., 2018; Wanyama et al., 2019; Zhao et al., 2019). Warming increased net soil CH_4 uptake from ~87.50 to ~98.28 % when including both summer campaigns (Table 3), which also improved the correlation with soil moisture ($R^2_{Control} = 0.12$, $R^2_{Warming} = 0.24$; Fig. 5c, Table 4c). However, neither the increase in net soil CH_4 uptake and nor marginally drier soil conditions under the realized warming were statistically significant (Fig. 2, Fig. 3, Table 1, Table 2, Table 3b), and sensitivity of soil CH_4 effluxes to soil moisture were statistically undistinguishable between Warming and Control plots (Fig. 5c, Table 4c, Table SM5.3). Furthermore, soil moisture differences remained relatively similar between treatments (Fig. 4) even during days when net CH_4 uptake was stronger in the Warming plots (Fig. 4). Together, our results indicate that soil moisture exerts a consistent control on soil CH_4 dynamics across treatments, while short term directional shifts under warming likely reflect processes beyond soil abiotic conditions alone.

Consistent with this interpretation, variability in soil CH_4 fluxes was largely driven by sampling day variation, whereas the warming manipulation did not exert a significant overall effect (sampling day; GAMM $p < 0.001$; Fig. 4; Tables 3b, Fig. SM3.2; SM3.3b, SM3.4b, SM3.5b). Across both summer campaigns, Control and Warming treatments exhibited similar soil CH_4 flux trajectories, with a brief shift toward higher net soil CH_4 uptake under warming during the wetter summer 2023, (July 7–24; Fig. 2, Fig. 4, Table SM4). Outside this window, soil CH_4 fluxes were virtually indistinguishable between treatments during the remaining summer 2023 sampling dates and throughout the drier summer campaign in 2024 (Fig. 2, Fig. 4, Table SM4). In contrast, variability across sampling days had no effect on soil CO_2 fluxes (GAMMs $p > 0.05$), which were consistently higher under Warming treatment in summer campaign 2023 and comparable between treatments in summer field campaign 2024 (Fig. 4, Table SM4, Table SM3.3a, Table SM3.4a, Table SM3.5a). Together, these results suggest the directional shifts in net CH_4 uptake under warming conditions were event–driven contingent on specific environmental and biotic processes rather than reflecting a persistent treatment effect. We suggest that these patterns may reflect interactive effects of warming and transient increase of nutrient availability that modulate soil GHG fluxes under contrasting hydrological regimes (i.e., wet *vs.* drier summers), which differentially regulated soil respiration and net CH_4 uptake across treatments.

To evaluate the mechanisms underlying these episodic shifts in net CH_4 uptake under warming, one may consider whether transient enhancements in root–derived carbon inputs, in other words, rhizodeposition, could account for the observed patterns. However, this mechanism is unlikely to explain our results given the documented decline in root biomass at TRACE under warming and post–hurricane recovery over five years of experimental manipulation (Tunison et al., 2024; Yaffar et al., 2021). Warming (Heinzle et al., 2023) and optimal precipitation regimes (Li et al., 2004) augment fine root biomass and enhance exudation of labile C compounds and inorganic nitrogen (N), which can stimulate heterotrophic activity, and, in turn methanotrophy, resulting into a positive correlation between soil respiration rates and net CH_4 uptake (Tveit et al., 2019; Veldkamp et al., 2013; Voigt et al., 2023). Although we observed such coupling between soil respiration and net CH_4 uptake (Fig. 6, Table 5, Table SM5.1), roots under warming and post–hurricane at TRACE acclimated by reducing biomass and fine–root production rather than increasing metabolic activity (Tunison et al., 2024; Yaffar et al., 2021). This points to curtailed, or at least no shifts, in exudation rates. Consequently, changes in rhizodeposition rates cannot explain the pronounced enhancement of CH_4 uptake under warming treatment during brief periods in summer 2023 nor its decline across the remaining sampling days in both summer campaigns.

In summary, our observations highlight the complexity of interpreting soil CH_4 flux dynamics in tropical forests, which cannot be explained by variation in abiotic factors alone. Instead, integrating biogeochemical processes across multiple pools can better constrain the balance between methane uptake and emission in soils. Overall, our data indicate that net CH_4 uptake was positively correlated with soil respiration in both treatments (Fig. 6, Table SM6). Given the lower contribution of roots to total soil respiration under warming conditions (Tunison et al., 2024), the increase in soil respiration observed during the summer 2023 campaign was likely mediated by enhanced decomposition rates, which have likely stimulated methanotrophic activity, at least during a short time window in summer 2023 (McFarlane et al., 2024; Nottingham et al., 2020) that also contributed to CO_2 production (Nazaries et al., 2013). Supporting this interpretation, extractable C and NO_3^-, as well as microbial C and N, were higher under warming following two years of hurricane–disturbance recovery compared to unwarmed plots (Reed et al., 2020). In contrast, the absence of significant treatment effects during the summer campaign 2024 may reflect the reduced frequency of rainfall events (Fig. 2; Table SM1.2), which limited litter–leached, labial nutrient fluxes and constrained the warming response on soil GHG fluxes (Deng et al., 2018). Nevertheless, with our current dataset it remains unclear which mechanism primarily drove such transient increase of net CH_4 uptake in the Warming plots relative to the Control, or why net CH_4 uptake declined in warmer plots during part of summer 2023 and the summer 2024 campaigns. The apparent decline in CH_4 uptake capacity across both summer campaigns may also reflect the smaller sample size and shorter temporal coverage (Fig. 3c–d, Fig. 4b, Fig. 5d, Fig. 6, Fig. SM2.4c–d, Table 3, Table SM4), which could have limited our ability to capture potential shifts toward greater or reduced CH_4 sink strength. Despite these uncertainties, our targeted study suggests that the soil buffering capacity against CH_4 emissions at TRACE remains largely unaltered under warming and during long–term post–hurricane recovery, including wet periods.

4.3. Disturbance legacy effect of hurricanes are diluted

The TRACE site offered a unique opportunity to test the effects of warming on net soil GHG fluxes and to assess whether disturbance legacies from Hurricanes Irma and Maria persisted and were exacerbated under a warming scenario. Our results indicate that lowland tropical forest soils in Puerto Rico remained a substantial CH_4 sink even under warmed conditions. Overall, the realized warming was sufficient to boost soil respiration rates, at least during the summer campaign 2023, but not enough to enhance net CH_4 uptake. Altered methane metabolism was observed only during a brief period in summer campaign 2023, as indicated by higher net CH_4 uptake and higher soil respiration rates relative to the Control treatment, reflecting shifts toward enhanced methanotrophic activity. Yet such changes cannot be fully explained by warmer and marginally drier soil conditions as predicted in our hypothesis (1), suggesting that biological factors, potentially shifts in microbial community composition or activity, should be considered to explain this shift toward higher methanotrophic activity dynamics under different treatments. Although warming did not alter soil moisture levels in warmed plots (Table 1), soil conditions were oxygenated enough to promote methane uptake rather than emission in both Control and Warming treatments (Figs. 3c–d, 4b, 5c–d). Previous studies reported a temporary switch to net CH_4 emission for about seven months following Hurricanes Maria and Irma (Quebbeman et al., 2022a), when litterfall and fallen branches, combined with reduced evapotranspiration and high throughfall, maintained high soil moisture by reducing soil exposure to air. Prolonged wet conditions following hurricane recovery, coupled with warming–induced stimulation of microbial activity, could theoretically sustain longer–term methane emissions (hypothesis (2)). However, sustained anoxic conditions generally decline as forests recover after such disturbances (Vargas, 2012). Indeed, the forest canopy in the LEF recovered within two years after the hurricanes (Reed et al., 2020), likely facilitating oxygenation in the topsoil where methanotrophs live by reducing throughfall and increasing evapotranspiration (Shiels et al., 2014). Therefore, we fully reject our alternative hypothesis (2) and suggest that the hurricane effect on soil GHG has been diluted as the forest recovers.

4.4. Emissions of methane are rare or limited to localized topographic concavities

Despite tropical forests at TRACE functioning as an overall CH_4 sink, occasional net CH_4 emissions were also observed. Positive fluxes measured during the summer campaigns, although rare, represent “hot moments” of net CH_4 emissions, here identified as outliers of efflux distributions (Fig. 3c-d, Fig. SM3.2c) (O’Connell et al., 2018; Sihi et al., 2021). These events likely reflect rapid redox shifts under intermediate to elevated soil moisture that suppressed methanotrophic activity and respiration rates (Barcellos et al., 2018; Huang and Hall, 2017), which is consistent with our observations (Fig. 5, Fig. 6).

Notably, soil CH_4 fluxes and moisture displayed modest but meaningful spatial variability (Table 1, Table 2), with the largest random variance attributed to plot–level differences (GAMMs $p < 0.001$; Fig. 3c-d, Table 3, Table SM3.3, Table SM3.4, Table 3.5), and only minor variability explained by collar ID for CH_4 fluxes (GAMMs $p < 0.001$; Table 3, Fig. SM3.2c–d, Table SM3.3, Table SM3.4, Table 3.5). This suggests that local spatial heterogeneity can either modulate CH_4 uptake or create conditions for net emissions (O’Connell et al., 2018; Quebbeman et al., 2022b; Sihi et al., 2021). One striking example occurred in Plot 5, where especially collar U8 consistently produced positive CH_4 fluxes (Fig. SM2.4c). Comparison of variance components from GAMMs fitted to the 2023 and 2024 summer campaigns (Table 3b), including a reduced model excluding Plot 5, indicates that this plot contributes 30.30 % of the total soil CH_4 flux variability across the TRACE site. This disproportionate impact of a localized “hot spot” likely contributes to the apparent bimodal distribution of soil CH_4 fluxes in Control plots (Fig. 3c). This anomaly appears to be linked to local topographic and textural controls that create unique hydrological and biogeochemical conditions (Barcellos et al., 2018; O’Connell et al., 2018). This plot lies on a gentle slope (16°; Kimball et al., 2018), with collars U8 and U9 positioned close to each other on a flat step near the center of Plot 5. This localized concave topography, combined with the poorly drained, clay–rich colluvium and weathered material included in these soils (Beinroth et al., 2003; Muñoz et al., 2018; Ping et al., 2013), likely foster conditions favorable for CH_4 emission, at least in collar U8. Such topographically driven water accumulation likely created a local “hot spot” for CH_4 emissions by maintaining high soil moisture and low oxygen availability in potential anoxic microsites (O’Connell et al., 2018; Quebbeman et al., 2022b, 2022a; Sihi et al., 2021). Supporting this interpretation, Plot 5 was among the wettest measured, with median soil moisture values of 38.65 % in 2023 and 44.94 % from January–July 2024, respectively (Fig. SM1.2). This localized CH_4–emitting microsite likely contributed to the higher linear coefficients and weaker correlations observed in the respiration–CH_4 relationship. In other words, while low to intermediate soil CO_2 respiration rates in Control plots typically coincided with net CH_4 uptake, equivalent respiration rates in the Warming plot more often aligned with net CH_4 sink (Fig. 6, Table 5, Table SM6).

Importantly, such hot spots for methanogenesis may respond differently to warming than better–drained soils. While warming generally enhanced soil CH_4 uptake across most plots, localized concavities with persistently high moisture may remain buffered against warming–induced aeration or even experience enhanced CH_4 emission if warming accelerates decomposition under anaerobic conditions (Das and Adhya, 2012). This spatial and temporal heterogeneity in soil CH_4 emission likely contributes to the weak and inconsistent treatment effects observed for CH_4 fluxes at the plot scale, despite clear warming effects on soil respiration (GAMMs $p = 0.03$; Fig. 3a-b, Fig. 4a, Table 2, Table 3a, Table SM3.4a).

Most global CH_4 budget estimates derived from satellite inversions and atmospheric models operate at relatively coarse spatial resolutions (e.g., Feng et al., 2022; Saunois et al., 2020, 2025). While these approaches capture broad regional patterns in atmospheric CH_4 concentrations, they often cannot explicitly resolve fine–scale heterogeneity in soil–atmosphere CH_4 fluxes driven by local topographic and hydrological controls. As a result, localized "hot spots" of soil CH_4 emissions, such as those associated with concave, poorly drained microsites are typically underrepresented or averaged out in regional and global flux estimates. In this study, a single plot (Plot 5) contributed 30.30% of the total soil CH_4 flux variability across the TRACE site when accounting for both summer campaigns, highlighting how strongly such fine-scale heterogeneity can influence ecosystem-scale estimates. Only a limited number of studies in lowland tropical forests explicitly account for the influence of fine–scale topographic and hydrological variability on soil CH_4 dynamics (e.g., O'Connell et al., 2018; Quebbeman et al., 2022a, b; Sihi et al., 2021, this study). Failure to represent this heterogeneity may bias estimates of tropical soil CH_4 exchange, particularly under future climate scenarios that alter precipitation regimes, soil moisture distributions, and the frequency of extreme wetting events. Our observation of persistent, plot–specific CH_4 emissions at TRACE highlights how localized hydrological settings can disproportionately contribute to flux variability and underscores the importance of incorporating sub–grid heterogeneity into models of the global CH_4 budget.

Taken together, these findings suggest that while CH_4 emissions in this lowland tropical soil are rare, they can emerge under rapid rewetting or particular topographic/hydrological settings (Barcellos et al., 2018; O'Connell et al., 2018). This pattern aligns with observations from other tropical forest sites, which emphasize the buffering capacity of lowland tropical soils as reservoirs for atmospheric CH_4, including in Australia (Kiese et al., 2008), Brazil (Keller et al., 2005), China (Beinroth et al., 2003; Fang et al., 2010; Muñoz et al., 2018; Zhao et al., 2019), Congo (Barthel et al., 2022), Costa Rica, and Panama (Veldkamp et al., 2013).

4.5. Do lowland tropical forests in Puerto Rico thermally acclimate under prolonged warming?

A central challenge posed by ongoing global warming is to determine whether soil respiration across ecosystems will acclimate to novel climatic conditions and, if so, to what extent it can sustain resilience. Over the past decades, numerous experimental warming manipulations have sought to address this challenge by testing the sensitivity of soil respiration to temperature increases (Bradford et al., 2008; Carey et al., 2016; Melillo et al., 2017). Results across ecosystems have been mixed: warmed plots have shown no, partial, or full thermal acclimation of soil respiration. Such responses are often evaluated by the magnitude (intercept) and the shape (linear and quadratic slopes) of the soil CO_2–temperature response curve. In principle, higher temperatures should stimulate higher respiration rates (Bradford et al., 2008; Carey et al., 2016; Melillo et al., 2017). Thermal acclimation, however, is inferred when warming produces only slightly higher or no change in respiration rates compared with Control plots, or even lower CO_2 fluxes at a given temperature, resulting in response curves with equal or lower intercepts and shallower slopes compared to controls (Bradford et al., 2008; Carey et al., 2016; Melillo et al., 2017). At TRACE, after one year (Wood et al., 2025) and six to seven years (this study) of prolonged warming, we observed a distinct pattern: soil respiration under warming showed a higher intercept but lower slope compared to controls (Fig. 5b, Table 4, Table SM5.2). This suggests that while baseline respiration is elevated, the sensitivity of respiration to further temperature increases is reduced, even when warming is constrained to $\sim+1.95^{\circ}$C (e.g., this study) relative to the targeted $+4^{\circ}$C treatment (Wood et al., 2025).

A similar pattern emerged for CH_4 uptake: in control plots, net soil CH_4 uptake significantly increased as soil temperature within 0–10 cm depth increased, whereas under warming, the CH_4 uptake response was enhanced but plateaued, showing a significant but low correlation with soil temperature close to 0 (Fig. 5d, Table 4, Table SM5.4). These results are also consistent with field observations from other lowland tropical forest soils (e.g., lowland tropical forest sites in China and Africa), where soil CH_4 uptake remains the dominant flux process even under modest variations in soil temperature (Wanyama et al., 2019; Zhao et al., 2019). Given the moderate correlation between CO_2 and CH_4 responses (Fig. 6), we hypothesize that this response may point to a low upregulation of methanotrophic activity under warming, consistent with observations that heterotrophic microbes in low–latitude tropical forests, including methanotrophs, already operate near their optimal temperature and thus show reduced sensitivity to further warming (Jiang et al., 2025; Nottingham et al., 2020). Recent work on methanotrophs adapted to high–temperature environments suggests that cells can maintain high CH_4 oxidation efficiency even as growth slows, effectively sacrificing proliferation to sustain CH_4 uptake (Tveit et al., 2023). Moreover, lowland tropical forests may have more abundance in generalist methanotrophs, such those of the genus *Methylocystis*, that adapt to a wide range of temperature condition, further supporting low shifts in CH_4 oxidation rates (Gontijo et al., 2024). While we do not have microbial community composition or enzymatic activity data from TRACE to further support thermal acclimation patterns, these mechanisms may reasonably explain our observations, where methanotrophic activity appears to remain stable at higher temperatures (Fig. 5d, Table 4, Table SM5.4).

If this were the case, whether this response represents sustained acclimation or a transient adjustment cannot be resolved given the temporal scope of our dataset. We collected this dataset during two consecutive calendar summers (Fig. 2) to evaluate the vulnerability of soil CH_4 uptake to increasing average soil moisture during months over which wetter and warmer periods are likely, conditions that could promote methanogenesis rather than net CH_4 uptake under elevated precipitation and higher moisture levels. In both field campaigns (summer 2023 and 2024), lowland tropical forests at TRACE remained an important CH_4 sink under experimental warming and post–hurricane recovery, and no reduction in net CH_4 strength was observed between treatments and across both summer campaigns (Figs. 3b, Fig. 4b, Table 2, Table 3; Supplementary Materials SM2 and SM4). However, our measurements cannot capture responses to cumulative annual warming or during other months with different combinations of temperature and rainfall amount. Previous studies have demonstrated that the temperature sensitivity of soil biogeochemical processes in subtropical forests, including respiration, can vary substantially across monthly timescales under experimental warming (Machmuller et al., 2018). Accordingly, the reduced temperature sensitivity on soil CH_4 uptake observed under experimental warming at TRACE may reflect a seasonal or short–term acclimation response rather than sustained, year–round response. Longer, year–round observations would allow for determination of whether this response persists or shifts, particularly under ongoing warming and increasing hurricane disturbance frequency and intensity.

Since 1876, high-energy storms (e.g., category 3-5) have been dominant components of disturbance for tropical forests in Puerto Rico, with an average recurrence interval of ~14 years between major events (Zimmerman et al., 2020). Projections indicate that by the mid–21st century, strong hurricanes in the North Atlantic area, including the island, may increase in intensity by ~36% percent and in frequency by ~19% under a ~4 °C warming scenario (Lopez et al., 2024). Strong hurricanes can remove nearly 50% of aboveground biomass (Scatena et al., 1996), while lowland tropical forests typically recover canopy structure within approximately two years following disturbance (Shiels et al., 2014). Consequently, shorter intervals between intense hurricane events could lead to more frequent inputs of fresh litter over large areas, as well as repeated periods of reduced evapotranspiration, soil anoxia, and associated shifts on biogeochemical cycling (Reed et al., 2020;

Shiels et al., 2014; Uriarte et al., 2019). Field measurements following hurricanes María and Irma documented a shift from net CH_4 uptake to net emission driven by altered soil redox conditions, persisting for at least seven months after the events (Quebbeman et al., 2022a). Together, these processes suggest that the interaction between warming and increasing hurricane disturbance may make the capacity of lowland tropical forests to act as CH_4 sinks more variable over time.

5. Conclusions

Overall, our observations indicate that lowland tropical forests in Puerto Rico remain net soil CH_4 sink during wet conditions, even under prolonged experimental warming following years of major hurricane disturbance. Despite achieving only modest soil warming (~1.95°C), warming altered soil greenhouse gas dynamics in temporally dependent ways, enhancing soil respiration during one of the two summer campaigns but did not substantially alter net CH_4 uptake strength across treatments. Reduced temperature sensitivity of both soil respiration and CH_4 uptake under warming suggests a potential attenuation of microbial responses at higher soil temperatures, possibly reflecting operation near thermal optima in these tropical ecosystems. The consistent coupling between soil CO_2 efflux and CH_4 uptake further indicates that methanotrophic activity is closely linked to heterotrophic decomposition. Finally, finer–scale temporal and spatial variability in soil CH_4 effluxes suggest that soil CH_4 dynamics are modulated by interactive biotic and environmental drivers rather than by soil temperature and soil moisture variation alone.

Together, these findings point to a short–term resilience of soil CH_4 dynamics to warming in lowland tropical forests, yet our observations are limited to calendar summer months. It remains unclear whether this apparent response of soil CH_4 dynamics to warming represents a sustained adjustment or a transient, seasonally constrained response. Longer–term, multi–season observations, integrated with microbial community composition and nutrient dynamics, would be valuable to determining whether continued warming and increasing hurricane disturbance frequency may eventually weaken soil CH_4 sink strength or promote persistent transitions toward net CH_4 emissions.

Funding sources

This research was supported by the US Department of Energy, Office of Science, Office of Biological and Environmental Research Dept of Energy (DE-SC-0012000, DE-SC0011806, DE-SC0025314, 89243018S-SC-000014, 89243018S-SC-000017, DE-SC0018942, DE-SC0022095, 89243021S-SC-000076) to M.A.C., S.C.R., D.S., and T.E.W.; a National Science Foundation award (DEB-1754713) to M.A.C., S.C.R., and T.E. W.; a National Science Foundation award to C.S.O. (DEB-2437445); Macalester College; Chapman University; USDA Forest Service International Institute of Tropical Forestry; and the University of Puerto Rico-Rio Piedras. R.C.P. was supported by a USDA National Needs Fellowship from NIFA (Grant 2019-38420-28979) and by the NSF National Research Trainee Program LandscapeU (DGE 1828822). L.Z., N.B.S., H. P.C, T.D, and M.K. were supported by Macalester College Collaborative Summer Research (CSR) Fellowship Awards.

Data availability

All spreadsheets (e.g., soil flux data, microclimate data, soil abiotic variable data) and code used for the production of this manuscript are archived in the Environmental System Science Data Infrastructure for a Virtual Ecosystem (ESS-DIVE) Database in Larocca Conte et al. (2026; dataset DOI: 10.15485/3001415).

CRediT authorship contribution statement

Gabriele Larocca Conte: Writing – review & editing, Writing – original draft, Visualization, Validation, Supervision, Software, Resources, Methodology, Investigation, Formal analysis, Data curation, Conceptualization. **Lucia Zuvela:** Writing – review & editing, Visualization, Validation, Software, Methodology, Investigation, Formal analysis, Data curation, Conceptualization. **Rachel Cruz-Pérez:** Visualization, Supervision, Methodology, Investigation, Data curation. **Tatiana Barreto-Vélez:** Writing – review & editing, Supervision, Resources, Project administration. **Nibia Becerra-Santillan:** Visualization, Methodology, Investigation, Data curation, Conceptualization. **Sophia F. Campbell:** Visualization, Methodology, Investigation, Data curation, Conceptualization. **Hieu P. Chu:** Methodology, Investigation, Data curation, Conceptualization. **Trung Dam:** Methodology, Investigation, Data curation, Conceptualization. **Iana F. Grullón-Penkova:** Writing – review & editing, Supervision, Resources, Project administration. **Miriam Kleit:** Writing – review & editing, Visualization, Methodology, Investigation, Data curation, Conceptualization. **Deyaneira A. Ortiz-Iglesias:** Writing – review & editing, Supervision, Resources, Project administration. **Laura C. Rubio-Lebrón:** Writing – review & editing, Supervision, Resources, Project administration. **Molly A. Cavaleri:** Writing – review & editing, Visualization, Validation, Supervision, Resources, Project administration, Funding acquisition. **Sasha C. Reed:** Writing – review & editing, Visualization, Validation, Supervision, Resources, Project administration, Funding acquisition. **Debjani Sihi:** Writing – review & editing, Visualization, Validation, Supervision, Resources, Project administration, Funding acquisition. **Tana E. Wood:** Writing – review & editing, Visualization, Validation, Supervision, Resources, Project administration, Funding acquisition. **Christine S. O'Connell:** Writing – review & editing, Visualization, Validation, Supervision, Software, Resources, Project administration, Methodology, Investigation, Funding acquisition, Formal analysis, Data curation, Conceptualization.

Declaration of competing interest

The authors declare the following financial interests/personal relationships which may be considered as potential competing interests:

Molly A. Cavaleri reports financial support was provided by US Department of Energy. Sasha C. Reed reports financial support was provided by US Department of Energy. Debjani Sihi reports financial support was provided by US Department of Energy. Tana E. Wood reports financial support was provided by US Department of Energy. Molly A. Cavaleri reports financial support was provided by National Science Foundation. Sasha C. Reed reports financial support was provided by National Science Foundation. Tana E. Wood reports financial support was provided by National Science Foundation. Christine S. O'Connell reports was provided by National Science Foundation. Rachel Cruz-Perez reports was provided by National Institute of Food and Agriculture. Rachel Cruz-Perez reports financial support was provided by National Science Foundation. If there are other authors, they declare that they have no known competing financial interests or personal relationships that could have appeared to influence the work reported in this paper.

Acknowledgements

This research was conducted at the TRACE site, located next to the Sabana Field Research Station in the El Yunque National Forest, with the assistance of numerous interns and volunteers who contributed to data collection for this manuscript. We are deeply grateful to past and present TRACE project managers—Aura Alonso-Rodríguez, Megan Berberich, and Isabel Loza Rivera—and TRACE and USGS technicians—William Mejía-García, Nicole Gutiérrez Ramos, Armin Howell, and Robin Reibold—whose support was essential to the success of the TRACE project. This work was supported by Macalester College, St. Paul, Minnesota, USA and, most recently, Chapman University, Orange, California, USA and the University of Puerto Rico. This work was also supported by the

USDA Forest Service International Institute of Tropical Forestry. Any use of trade, firm, or product names is for descriptive purposes only and does not imply endorsement by the U.S. Government.

Finally, we are deeply thankful to the two anonymous reviewers for their insightful and constructive comments, which significantly improved the quality of this manuscript.

Supplementary materials

Supplementary material associated with this article can be found, in the online version, at doi:10.1016/j.agrformet.2026.111225.

References

Auguie, B., Antonov, A., 2017. gridExtra: miscellaneous functions for “Grid” graphics. R package version 2.3. https://CRAN.R-project.org/package=gridExtra.

Barcellos, D., O’connell, C.S., Silver, W., Meile, C., Thompson, A., 2018. Hot spots and hot moments of soil moisture explain fluctuations in iron and carbon cycling in a humid tropical forest soil. Soil. Syst. 2, 59. https://doi.org/10.3390/soilsystems2040059, 2018, Vol. 2, Page 59.

Barthel, M., Bauters, M., Baumgartner, S., Drake, T.W., Bey, N.M., Bush, G., Boeckx, P., Botefa, C.I., Dériaz, N., Ekamba, G.L., Gallarotti, N., Mbayu, F.M., Mugula, J.K., Makelele, I.A., Mbongo, C.E., Mohn, J., Mandea, J.Z., Mpambi, D.M., Ntaboba, L.C., Rukeza, M.B., Spencer, R.G.M., Summerauer, L., Vanlauwe, B., Van Oost, K., Wolf, B., Six, J., 2022. Low N2O and variable CH4 fluxes from tropical forest soils of the Congo Basin. Nat. Commun. 13, 1–8. https://doi.org/10.1038/s41467-022-27978-6.

Beinroth, F.H., Engel, R.J., Lugo, J.L., Santiago, C.L., Ríos, S., Brannon, G.R., 2003. Updated classification of the soils of Puerto Rico, 2002. University of Puerto Rico Mayagüez. Bulletin 303, 1–73.

Bolker, B., Robinson, D., 2024. broom.mixed: tidying methods for mixed models. R package version 0.2.9.7. https://github.com/bbolker/broom.mixed.

Bonan, G.B., 2008. Forests and climate change: forcings, feedbacks, and the climate benefits of forests. Science 320 (5882), 1444–1449. https://doi.org/10.1126/science.1155121.

Bradford, M.A., Davies, C.A., Frey, S.D., Maddox, T.R., Melillo, J.M., Mohan, J.E., Reynolds, J.F., Treseder, K.K., Wallenstein, M.D., 2008. Thermal adaptation of soil microbial respiration to elevated temperature. Ecol. Lett. 11, 1316–1327. https://doi.org/10.1111/J.1461-0248.2008.01251.X.

Campbell, G.S., 1985. Soil Physics with BASIC: Transport Models for Soil-Plant Systems, 1st ed. Elsevier, Amsterdam.

Carey, J.C., Tang, J., Templer, P.H., Kroeger, K.D., Crowther, T.W., Burton, A.J., Dukes, J.S., Emmett, B., Frey, S.D., Heskel, M.A., Jiang, L., Machmuller, M.B., Mohan, J., Panetta, A.M., Reich, P.B., Reinschj, S., Wang, X., Allison, S.D., Bamminger, C., Bridgham, S., Collins, S.L., De Dato, G., Eddy, W.C., Enquist, B.J., Estiarte, M., Harte, J., Henderson, A., Johnson, B.R., Larsen, K.S., Luo, Y., Marhan, S., Melillo, J.M., Peñuelas, J., Pfeifer-Meister, L., Poll, C., Rastetter, E., Reinmann, A.B., Reynolds, L.L., Schmidt, I.K., Shaver, G.R., Strong, A.L., Suseela, V., Tietema, A., 2016. Temperature response of soil respiration largely unaltered with experimental warming. Proc. Natl. Acad. Sci. U.S.A. 113, 13797–13802. https://doi.org/10.1073/pnas.1605365113.

Castro, M.S., Steudler, P.A., Melillo, J.M, Aber, J.D., Bowden, R.D., 1995. Factors controlling atmospheric methane consumption by temperate forest soils. Glob. Biogeochem. Cycles 9, 1–10. https://doi.org/10.1029/94GB02651.

Cavaleri, M.A., Reed, S.C., Smith, W.K., Wood, T.E., 2015. Urgent need for warming experiments in tropical forests. Glob. Chang. Biol. 21, 2111–2121. https://doi.org/10.1111/gcb.12860.

Chambers, J.Q., Tribuzy, E.S., Toledo, L.C., Crispim, B.F., Higuchi, N., Dos Santos, J., Araújo, A.C., Kruijt, B., Nobre, A.D., Trumbore, S.E., 2004. Respiration from a tropical forest ecosystem: partitioning of sources and low carbon use efficiency. Ecol. Appl. 14. https://doi.org/10.1890/01-6012.

Collins, M., Knutti, R., Arblaster, J., Dufresne, J.-L., Fichefet, T., Friedlingstein, P., Gao, X., Gutowski, W.J., Johns, T., Krinner, G., Shongwe, M., Tebaldi, C., Weaver, A. J., Wehner, M., 2013. Long-term climate change: projections, commitments and irreversibility. In: Stocker, T.F., Qin, D., Plattner, G.-K., Tignor, M., Allen, S.K., Boschung, J., Nauels, A., Xia, Y., Bex, V., Midgley, P.M. (Eds.), Climate Change 2013 the Physical Science Basis: Working Group I Contribution to the Fifth Assessment Report of the Intergovernmental Panel on Climate Change. Cambridge University Press, Cambridge and New York, pp. 1029–1136. https://doi.org/10.1017/CBO9781107415324.024.

Conrad, R., 2020. Importance of hydrogenotrophic, aceticlastic and methylotrophic methanogenesis for methane production in terrestrial, aquatic and other anoxic environments: a mini review. Pedosphere 30, 25–39. https://doi.org/10.1016/S1002-0160(18)60052-9.

Corteselli, E.M., Burtis, J.C., Heinz, A.K., Yavitt, J.B., 2017. Leaf litter fuels methanogenesis throughout decomposition in a forested peatland. Ecosystems 20, 1217–1232. https://doi.org/10.1007/s10021-016-0105-9.

Das, S., Adhya, T.K., 2012. Dynamics of methanogenesis and methanotrophy in tropical paddy soils as influenced by elevated CO2 and temperature interaction. Soil. Biol. Biochem. 47, 36–45. https://doi.org/10.1016/j.soilbio.2011.11.020.

de Gerenyu, V.O.L., Kurbatova, Y.A., Kurganova, I.N., Tiunov, A.V., Anichkin, A.Y., Myakshina, T.N., Kuznetsov, A.N., 2011. Daily and seasonal dynamics of CO2 fluxes from soils under different stands of monsoon tropical forest. Eurasian Soil Sci. 44, 984–990. https://doi.org/10.1134/S1064229311090067, 2011 44:9.

Deng, Q., Zhang, D., Han, X., Chu, G., Zhang, Q., Hui, D., 2018. Changing rainfall frequency rather than drought rapidly alters annual soil respiration in a tropical forest. Soil. Biol. Biochem. 121, 8–15. https://doi.org/10.1016/j.soilbio.2018.02.023.

Dijkstra, F.A., Morgan, J.A., Von Fischer, J.C., Follett, R.F., 2011. Elevated CO2 and warming effects on CH4 uptake in a semiarid grassland below optimum soil moisture. J. Geophys. Res. Biogeosci. 116, 1007. https://doi.org/10.1029/2010JG001288.

D’Imperio, L., Nielsen, C.S., Westergaard-Nielsen, A., Michelsen, A., Elberling, B., 2017. Methane oxidation in contrasting soil types: responses to experimental warming with implication for landscape-integrated CH4 budget. Glob. Chang. Biol. 23, 966–976. https://doi.org/10.1111/GCB.13400.

Dunnington, D., 2023. ggspatial: spatial data framework for ggplot2. R package version 1.1.10. https://paleolimbot.github.io/ggspatial/.

Dutaur, L., Verchot, L.V., 2007. A global inventory of the soil CH4 sink. Glob. Biogeochem. Cycles 21, 4013. https://doi.org/10.1029/2006GB002734.

Eaton, W.D., McGee, K.M., Alderfer, K., Jimenez, A.R., Hajibabaei, M., 2020. Increase in abundance and decrease in richness of soil microbes following Hurricane Otto in three primary forest types in the Northern Zone of Costa Rica. PLoS One 15, e0231187. https://doi.org/10.1371/JOURNAL.PONE.0231187.

Fang, H.J., Yu, G.R., Cheng, S.L., Zhu, T.H., Wang, Y.S., Yan, J.H., Wang, M., Cao, M., Zhou, M., 2010. Effects of multiple environmental factors on CO2 emission and CH4 uptake from old-growth forest soils. Biogeosciences 7, 395–407. https://doi.org/10.5194/BG-7-395-2010.

Feng, L., Palmer, P.I., Zhu, S., Parker, R.J., Liu, Y., 2022. Tropical methane emissions explain large fraction of recent changes in global atmospheric methane growth rate. Nat. Commun. 13, 1–8. https://doi.org/10.1038/s41467-022-28989-z.

Feng, X., Porporato, A., Rodriguez-Iturbe, I., 2013. Changes in rainfall seasonality in the tropics. Nat. Clim. Chang. 3, 811–815. https://doi.org/10.1038/nclimate1907, 2013 3:9.

Finn, D.R., Ziv-El, M., van Haren, J., Park, J.G., del Aguila-Pasquel, J., Urquiza–Muñoz, J. D., Cadillo-Quiroz, H., 2020. Methanogens and methanotrophs show nutrient-dependent Community assemblage patterns across tropical peatlands of the Pastaza-Marañón Basin, Peruvian Amazonia. Front. Microbiol. 11, 746. https://doi.org/10.3389/fmicb.2020.00746.

Forbrich, I., Kutzbach, L., Hormann, A., Wilmking, M., 2010. A comparison of linear and exponential regression for estimating diffusive CH4 fluxes by closed-chambers in peatlands. Soil. Biol. Biochem. 42, 507–515. https://doi.org/10.1016/j.soilbio.2009.12.004.

Fox, J., Weisberg, S., 2019. An R Companion to Applied Regression, 3rd ed. SAGE Publications, Inc., Thousand Oaks CA.

Frangi, J.L., Lugo, A.E., 1991. Hurricane damage to a flood plain forest in the Luquillo Mountains of Puerto Rico. Biotropica 23, 324. https://doi.org/10.2307/2388248.

García-Martinó, A.R., Warner, G.S., Scatena, F.N., Civco, D.L., 1996. Rainfall, runoff and elevation relationships in the Luquillo Mountains of Puerto Rico. Caribb. J. Sci. 32, 413–424.

Garnier, Simon, Ross, Noam, Rudis, Robert, Camargo, Pedro, A., Sciaini, Marco, Scherer, Cédric, 2023. viridis(Lite) - colorblind-friendly color maps for R. https://doi.org/10.5281/zenodo.4678327.

Gontijo, J.B., Paula, F.S., Bieluczyk, W., França, A.G., Navroski, D., Mandro, J.A., Venturini, A.M., Asselta, F.O., Mendes, L.W., Moura, J.M.S., Moreira, M.Z., Nüsslein, K., Bohannan, B.J.M., Bodelier, P.L.E., Rodrigues, J.L.M., Tsai, S.M., 2024. Methane-cycling microbial communities from Amazon floodplains and upland forests respond differently to simulated climate change scenarios. Environ. Microbiome 19, 1–19. https://doi.org/10.1186/s40793-024-00596-z.

González, G., Beusekom, A.E., Van Estrada, C.R., 2025. Luquillo Experimental Forest Sabana Weather Station Scaffold Tower 2018-2020 Data. Forest Service Research Data Archive. https://doi.org/10.2737/RDS-2021-0030-2.

Gould, W.A., Wadsworth, F.H., Quiñones, M., Fain, S.J., Álvarez-Berríos, N.L., 2018. . Shapefiles containing potential areas for agriculture, forestry, and conservation in Puerto Rico [dataset]. Forest Service Research Data Archive. https://doi.org/10.2737/RDS-2018-0004.

Grolemund, G., Wickham, H., 2011. Dates and times made easy with lubridate. J. Stat. Softw. 40, 1–25. https://doi.org/10.18637/jss.v040.i03.

Heartsill-Scalley, T., Scatena, F.N., Estrada, C., McDowell, W.H., Lugo, A.E., 2007. Disturbance and long-term patterns of rainfall and throughfall nutrient fluxes in a subtropical wet forest in Puerto Rico. J. Hydrol. 333, 472–485. https://doi.org/10.1016/J.JHYDROL.2006.09.019, 333, 472–485.

Heinzle, J., Liu, X., Tian, Y., Kwatcho Kengdo, S., Heinze, B., Nirschi, A., Borken, W., Inselsbacher, E., Wanek, W., Schindlbacher, A., 2023. Increase in fine root biomass enhances root exudation by long-term soil warming in a temperate forest. Front. For. Glob. Change 6, 1152142. https://doi.org/10.3389/ffgc.2023.1152142.

Hernangómez, D., 2023. Using the tidyverse with terra objects: the tidyterra package. J. Open. Source Softw. 8, 5751. https://doi.org/10.21105/joss.05751.

Hijmans, R.J., 2025a. terra: spatial data analysis. R package version 1.9-18. https://github.com/rspatial/terra.

Hijmans, R.J., 2025b. raster: geographic data analysis and modeling. R package version 3.6-32. https://CRAN.R-project.org/package=raster.

Holdridge, L.R., 1967. Life Zone Ecology. Tropical Science Center, San Jose.

Hollister, J., Shah, T., Nowosad, J., Robitaille, A.L., Beck, M.W., Johnson, M., 2023. elevatr: access elevation data from various APIs. https://doi.org/10.5281/zenodo.8335450.

Huang, W., Hall, S.J., 2017. Elevated moisture stimulates carbon loss from mineral soils by releasing protected organic matter. Nat. Commun. 8, 1–10. https://doi.org/10.1038/S41467-017-01998-z.

IPCC, 2018. Global warming of 1.5°C. An IPCC special report on the impacts of global warming of 1.5°C above pre-industrial levels and related global greenhouse gas emission pathways, in the context of strengthening the global response to the threat of climate change. https://doi.org/10.1038/291285a0.

Jiang, B., Chen, H., Wei, Z., Zhang, J., Guo, M., Yang, T., Zhou, X., 2025. Higher temperature sensitivity of forest soil methane oxidation in colder climates. Nat. Commun. 16, 1–9. https://doi.org/10.1038/S41467-025-57763-0.

Kassambara, A., 2023. ggpubr: "ggplot2" based publication ready plots.

Keller, M., Varner, R., Dias, J.D., Silva, H., Crill, P., De Oliveira, R.C., Asner, G.P., 2005. Soil–atmosphere exchange of nitrous oxide, nitric oxide, methane, and carbon dioxide in logged and undisturbed forest in the Tapajos National Forest, Brazil. Earth Interact. 9, 1–28. https://doi.org/10.1175/EI125.1.

Kiese, R., Wochele, S., Butterbach-Bahl, K., 2008. Site specific and regional estimates of methane uptake by tropical rainforest soils in north eastern Australia. Plant Soil. 309, 211–226. https://doi.org/10.1007/S11104-008-9545-0.

Kimball, B.A., Alonso-Rodríguez, A.M., Cavaleri, M.A., Reed, S.C., González, G., Wood, T. E., 2018. Infrared heater system for warming tropical forest understory plants and soils. Ecol. Evol. 8, 1932–1944. https://doi.org/10.1002/ECE3.3780.

Kirschbaum, M.U.F., 2006. The temperature dependence of organic-matter decomposition—still a topic of debate. Soil. Biol. Biochem. 38, 2510–2518. https://doi.org/10.1016/J.SOILBIO.2006.01.030.

Knutson, T., Camargo, S.J., Chan, J.C.L., Emanuel, K., Ho, C.H., Kossin, J., Mohapatra, M., Satoh, M., Sugi, M., Walsh, K., Wu, L., 2019. Tropical cyclones and climate change assessment: Part I: detection and attribution. Bull. Am. Meteorol. Soc. 100, 1987–2007. https://doi.org/10.1175/BAMS-D-18-0189.1.

Kuznetsova, A., Brockhoff, P.B., Christensen, R.H.B., 2017. lmerTest package: tests in linear mixed effects models. J. Stat. Softw. 82, 1–26. https://doi.org/10.18637/jss.v082.i13.

Lan, X., Thoning, K.W., Dlugokencky, E.J., 2025. Trends in Globally-Averaged CH4, N2O, and SF6 Determined from NOAA Global Monitoring Laboratory measurements. Version 2025-08. Global Monitoring Laboratory [data set].

Larocca Conte, G., Zuvela, L., Cruz-Pérez, R., Barreto-Vélez, T., Becerra-Santillan, N., Campbell, S., Chu, H., Dam, T., Grullón-Penkova, I., Kleit, M., Ortiz-Iglesias, D., Rubio-Lebrón, L., Cavaleri, M., Reed, S.C., Sihi, D., Wood, T., O'Connell, C., 2026. Data from: Lowland Tropical Forests Remain a Methane Sink Under Warming and Long-Term Hurricane Disturbance Recovery. Effects of Warming on Tropical Forest Carbon Cycling: Investigating Temperature Regulation of Key Tropical Tree and Soil Processes, ESS-DIVE repository. Dataset. doi:10.15485/3001415 accessed via https://data.ess-dive.lbl.gov/datasets/doi:10.15485/3001415 on 2026-05-07s.

Li, Y., Xu, M., Sun, O.J., Cui, W., 2004. Effects of root and litter exclusion on soil CO2 efflux and microbial biomass in wet tropical forests. Soil. Biol. Biochem. 36, 2111–2114. https://doi.org/10.1016/j.soilbio.2004.06.003.

Lodge, D.J., Scatena, F.N., Asbury, C.E., Sanchez, M.J., 1991. Fine litterfall and related nutrient inputs resulting from hurricane Hugo in subtropical wet and lower Montane rain forests of Puerto Rico. Biotropica 23, 336. https://doi.org/10.2307/2388249.

Lopez, H., Lee, S.K., West, R., Kim, D., Foltz, G.R., Alaka, G.J., Murakami, H., 2024. Projected increase in the frequency of extremely active Atlantic hurricane seasons. Sci. Adv. 10, 7856. https://doi.org/10.1126/sciadv.adq7856.

Ma, X., Jiang, S., Zhang, Z., Wang, H., Song, C., He, J.S., 2023. Long-term collar deployment leads to bias in soil respiration measurements. Methods Ecol. Evol. 14, 981–990. https://doi.org/10.1111/2041-210X.14056.

Machmuller, M.B., Ballantyne, F., Markewitz, D., Thompson, A., Wurzburger, N., Frankson, P.T., Mohan, J.E., 2018. Temperature sensitivity of soil respiration in a low-latitude forest ecosystem varies by season and habitat but is unaffected by experimental warming. Biogeochemistry 141, 63–73. https://doi.org/10.1007/s10533-018-0501-7, 2018 141:1.

Malhi, Y., Grace, J., 2000. Tropical forests and atmospheric carbon dioxide. Trends Ecol. Evol. 15, 332–337. https://doi.org/10.1016/S0169-5347(00)01906-6.

McFarlane, K.J., Cusack, D.F., Dietterich, L.H., Hedgpeth, A.L., Finstad, K.M., Nottingham, A.T., 2024. Experimental warming and drying increase older carbon contributions to soil respiration in lowland tropical forests. Nat. Commun. 15, 1–10. https://doi.org/10.1038/s41467-024-51422-6.

Melillo, J.M., Frey, S.D., DeAngelis, K.M., Werner, W.J., Bernard, M.J., Bowles, F.P., Pold, G., Knorr, M.A., Grandy, A.S., 2017. Long-term pattern and magnitude of soil carbon feedback to the climate system in a warming world. Science 358 (6359), 101–105. https://doi.org/10.1126/science.aan2874.

Muñoz, M.A., Lugo, W.I., Santiago, C., Matos, M., Ríos, S., Lugo, J., 2018. Taxonomic classification of the soils of Puerto Rico, 2017. Univ. Puerto Rico Mayagüez Bull. 313, 1–73.

Nazaries, L., Murrell, J.C., Millard, P., Baggs, L., Singh, B.K., 2013. Methane, microbes and models: fundamental understanding of the soil methane cycle for future predictions. Environ. Microbiol. 15, 2395–2417. https://doi.org/10.1111/1462-2920.12149.

Nisbet, E.G., Manning, M.R., Dlugokencky, E.J., Fisher, R.E., Lowry, D., Michel, S.E., Myhre, C.L., Platt, S.M., Allen, G., Bousquet, P., Brownlow, R., Cain, M., France, J.L., Hermansen, O., Hossaini, R., Jones, A.E., Levin, I., Manning, A.C., Myhre, G., Pyle, J. A., Vaughn, B.H., Warwick, N.J., White, J.W.C., 2019. Very strong atmospheric methane growth in the 4 years 2014–2017: implications for the Paris Agreement. Glob. Biogeochem. Cycles 33, 318–342. https://doi.org/10.1029/2018GB006009.

Nottingham, A.T., Meir, P., Velasquez, E., Turner, B.L., 2020. Soil carbon loss by experimental warming in a tropical forest. Nature 584, 234–237. https://doi.org/10.1038/S41586-020-2566-4.

Nottingham, A.T., Whitaker, J., Turner, B.L., Salinas, N., Zimmermann, M., Malhi, Y., Meir, P., 2015. Climate warming and soil carbon in tropical forests: insights from an elevation gradient in the Peruvian Andes. Bioscience 65, 906–921. https://doi.org/10.1093/BIOSCI/BIV109.

O'Connell, C.S., Ruan, L., Silver, W.L., 2018. Drought drives rapid shifts in tropical rainforest soil biogeochemistry and greenhouse gas emissions. Nat. Commun. 9, 1–9. https://doi.org/10.1038/s41467-018-03352-3.

Ooms, J., 2025. writexl: export data frames to excel "xlsx" format. R package version 1.5.4.9000. https://docs.ropensci.org/writexl/.

Pan, Y., Birdsey, R.A., Fang, J., Houghton, R., Kauppi, P.E., Kurz, W.A., Phillips, O.L., Shvidenko, A., Lewis, S.L., Canadell, J.G., Ciais, P., Jackson, R.B., Pacala, S.W., McGuire, A.D., Piao, S., Rautiainen, A., Sitch, S., Hayes, D., 2011. A large and persistent carbon sink in the world's forests. Science 333, 988–993. https://doi.org/10.1126/science.1201609.

Pebesma, E., 2018. Simple features for R: standardized support for spatial vector data. R. J. 10, 439–446. https://doi.org/10.32614/RJ-2018-009.

Pedersen, E.J., Miller, D.L., Simpson, G.L., Ross, N., 2019. Hierarchical generalized additive models in ecology: an introduction with mgcv. PeerJ. 7, e6876. https://doi.org/10.7717/peerj.6876.

Peltoniemi, K., Laiho, R., Juottonen, H., Bodrossy, L., Kell, D.K., Minkkinen, K., Mäkiranta, P., Mehtätalo, L., Penttilä, T., Siljanen, H.M.P., Tuittila, E.S., Tuomivirta, T., Fritze, H., 2016. Responses of methanogenic and methanotrophic communities to warming in varying moisture regimes of two boreal fens. Soil. Biol. Biochem. 97, 144–156. https://doi.org/10.1016/J.SOILBIO.2016.03.007.

Ping, C.-L., Michaelson, G.J., Stiles, C.A., González, G., 2013. Soil characteristics, carbon stores, and nutrient distribution in eight forest types along an elevation gradient, eastern Puerto Rico. Bulletins 67–86. https://doi.org/10.2307/26796806.

Posit team, 2025. RStudio: Integrated development environment for R [software]. Posit. Software, PBC. http://www.posit.co/.

Quebbeman, A.W., Menge, D.N.L., Arellano, G., Hall, J., Wood, T.E., Zimmerman, J.K., Uriarte, M., 2022a. A severe hurricane increases carbon dioxide and methane fluxes and triples nitrous oxide emissions in a tropical forest. Ecosystems 25, 1754–1766. https://doi.org/10.1007/S10021-022-00794-1.

Quebbeman, A.W., Menge, D.N.L., Zimmerman, J., Uriarte, M., 2022b. Topography and tree species improve estimates of spatial variation in soil greenhouse gas fluxes in a subtropical forest. Ecosystems 25, 648–660. https://doi.org/10.1007/s10021-021-00677-x.

Reed, S.C., Reibold, R., Cavaleri, M.A., Alonso-Rodríguez, A.M., Berberich, M.E., Wood, T.E., 2020. Soil biogeochemical responses of a tropical forest to warming and hurricane disturbance. Advances in Ecological Research. Academic Press, pp. 225–252. https://doi.org/10.1016/bs.aecr.2020.01.007.

Saunois, M., Martinez, A., Poulter, B., Zhang, Z., Raymond, P.A., Regnier, P., Canadell, J. G., Jackson, R.B., Patra, P.K., Bousquet, P., Ciais, P., Dlugokencky, E.J., Lan, X., Allen, G.H., Bastviken, D., Beerling, D.J., Belikov, D.A., Blake, D.R., Castaldi, S., Crippa, M., Deemer, B.R., Dennison, F., Etiope, G., Gedney, N., Höglund-Isaksson, L., Holgerson, M.A., Hopcroft, P.O., Hugelius, G., Ito, A., Jain, A.K., Janardanan, R., Johnson, M.S., Kleinen, T., Krummel, P.B., Lauerwald, R., Li, T., Liu, X., Mcdonald, K.C., Melton, J.R., Mühle, J., Müller, J., Murguia-Flores, F., Niwa, Y., Noce, S., Pan, S., Parker, R.J., Peng, C., Ramonet, M., Riley, W.J., Rocher-Ros, G., Rosentreter, J.A., Sasakawa, M., Segers, A., Smith, S.J., Stanley, E.H., Thanwerdas, J., Tian, H., Tsuruta, A., Tubiello, F.N., Weber, T.S., Van Der Werf, G. R., Worthy, D.E.J., Xi, Y., Yoshida, Y., Zhang, W., Zheng, B., Zhu, Qing, Zhu, Qiuan, Zhuang, Q., 2025. Global methane budget 2000-2020. Earth Syst. Sci. Data 17, 1873–1958. https://doi.org/10.5194/essd-17-1873-2025.

Saunois, M., Stavert, R., Poulter, A., Bousquet, B., Canadell, P., G., Jackson, J., B., Raymond, R., A., Dlugokencky, P., J., Houweling, E., Patra, S., K., Ciais, P., Arora, P., K., Bastviken, V., Bergamaschi, D., Blake, P., R., Brailsford, D., Bruhwiler, G., Carlson, L., M., Carrol, K., Castaldi, M., Chandra, S., Crevoisier, N., Crill, C., M., Covey, P., Curry, K., L., Etiope, C., Frankenberg, G., Gedney, C., Hegglin, N., I., Höglund-Isaksson, M., Hugelius, L., Ishizawa, G., Ito, M., Janssens-Maenhout, A., Jensen, G., M., Joos, K., Kleinen, F., Krummel, T., B., Langenfelds, P., L., Laruelle, R., G., Liu, G., MacHida, L., Maksyutov, T., McDonald, S., C., McNorton, K., Miller, J., A., Melton, P., R., Morino, J., Müller, I., Murguia-Flores, J., Naik, F., Niwa, V., Noce, Y., O'Doherty, S., Parker, S., J., Peng, R., Peng, C., Peters, S., P., Prigent, G., Prinn, C., Ramonet, R., Regnier, M., Riley, P., J., Rosentreter, W., A., Segers, J., Simpson, A., J., Shi, I., Smith, H., J., Paul Steele, S., Thornton, L., F., Tian, B., Tohjima, H., Tubiello, Y., N., Tsuruta, F., Viovy, A., Voulgarakis, N., Weber, A.S., Van Weele, T., Van Der Werf, M., R., Weiss, G., F., Worthy, R., Wunch, D., Yin, D., Yoshida, Y., Zhang, Y., Zhang, W., Zhao, Z., Zheng, Y., Zhu, B., Zhu, Qing, Qiuan, Zhuang, Q., 2020. The global methane budget 2000-2017. Earth Syst. Sci. Data 12, 1561–1623. https://doi.org/10.5194/essd-12-1561-2020.

Scatena, F.N., Larsen, M.C., 1991. Physical aspects of Hurricane Hugo in Puerto Rico. Biotropica 23, 317. https://doi.org/10.2307/2388247.

Scatena, F.N., Moya, S., Estrada, C., Chinea, J.D., 1996. The first five years in the reorganization of aboveground biomass and nutrient use following Hurricane Hugo in the Bisley Experimental Watersheds, Luquillo Experimental Forest, Puerto Rico. Biotropica 28, 424. https://doi.org/10.2307/2389086.

Shiels, A.B., González, G., Willig, M.R., 2014. Responses to canopy loss and debris deposition in a tropical forest ecosystem: synthesis from an experimental manipulation simulating effects of hurricane disturbance. For. Ecol. Manage 332, 124–133. https://doi.org/10.1016/J.FORECO.2014.08.005.

Sihi, D., Xu, X., Ortiz, M.S., O'Connell, C.S., Silver, W.L., López-Lloreda, C., Brenner, J. M., Quinn, R.K., Phillips, J.R., Newman, B.D., Mayes, M.A., 2021. Representing methane emissions from wet tropical forest soils using microbial functional groups constrained by soil diffusivity. Biogeosciences 18, 1769–1786. https://doi.org/10.5194/BG-18-1769-2021.

Silva, Z.S.J., Botta, S.B., Ana, P.A., França, C.M., Fernandes, K.P.S., Mesquita-Ferrari, R. A., Deana, A., Bussadori, S.K., 2015. Effect of papain-based gel on type I collagen - spectroscopy applied for microstructural analysis. Sci. Rep. 5, 1–7. https://doi.org/10.1038/srep11448.
Silver, W.L., Liptzin, D., Almaraz, M., 2013. Soil redox dynamics and biogeochemistry along a tropical elevation gradient. In: González, G., Willig, M.R., Waide, R.B. (Eds.), Ecological Gradient Analyses in a Tropical Landscape. Wiley-Blackwell, Hoboken, New Jersey, pp. 195–210.
Steudler, P.A., Melillo, J.M., Bowden, R.D., Castro, M.S., Lugo, A.E., 1991. The effects of natural and human disturbances on soil nitrogen dynamics and trace gas fluxes in a Puerto Rican wet forest. Biotropica 23, 356. https://doi.org/10.2307/2388252.
Townsend, A.R., Asner, G.P., Cleveland, C.C., 2008. The biogeochemical heterogeneity of tropical forests. Trends Ecol. Evol. 23, 424–431. https://doi.org/10.1016/J.TREE.2008.04.009.
Townsend, A.R., Cleveland, C.C., Houlton, B.Z., Alden, C.B., White, J.W.C., 2011. Multi-element regulation of the tropical forest carbon cycle. Front. Ecol. Environ. 9, 9–17. https://doi.org/10.1890/100047.
Tunison, R., Wood, T.E., Reed, S.C., Cavaleri, M.A., 2024. Respiratory acclimation of tropical forest roots in response to in situ experimental warming and hurricane disturbance. Ecosystems 27, 168–184. https://doi.org/10.1007/s10021-023-00880-y.
Tveit, A.T., Hestnes, A.G., Robinson, S.L., Schintlmeister, A., Dedysh, S.N., Jehmlich, N., Von Bergen, M., Herbold, C., Wagner, M., Richter, A., Svenning, M.M., 2019. Widespread soil bacterium that oxidizes atmospheric methane. Proc. Natl. Acad. Sci. U.S.A. 116, 8515–8524. https://doi.org/10.1073/PNAS.1817812116.
Tveit, A.T., Söllinger, A., Rainer, E.M., Didriksen, A., Hestnes, A.G., Motleleng, L., Hellinger, H.J., Rattei, T., Svenning, M.M., 2023. Thermal acclimation of methanotrophs from the genus methylobacter. ISME J. 17, 502–513. https://doi.org/10.1038/s41396-023-01363-7, 2023 17:4.
Uriarte, M., Thompson, J., Zimmerman, J.K., 2019. Hurricane María tripled stem breaks and doubled tree mortality relative to other major storms. Nat. Commun. 10, 1362-. https://doi.org/10.1038/s41467-019-09319-2, 2019 10:1.
Vargas, R., 2012. How a hurricane disturbance influences extreme CO2 fluxes and variance in a tropical forest. Environ. Res. Lett. 7, 035704. https://doi.org/10.1088/1748-9326/7/3/035704.
Veldkamp, E., Koehler, B., Corre, M.D., 2013. Indications of nitrogen-limited methane uptake in tropical forest soils. Biogeosciences 10, 5367–5379. https://doi.org/10.5194/BG-10-5367-2013.
Voigt, C., Virkkala, A.M., Hould Gosselin, G., Bennett, K.A., Black, T.A., Detto, M., Chevrier-Dion, C., Guggenberger, G., Hashmi, W., Kohl, L., Kou, D., Marquis, C., Marsh, P., Marushchak, M.E., Nesic, Z., Nykänen, H., Saarela, T., Sauheitl, L., Walker, B., Weiss, N., Wilcox, E.J., Sonnentag, O., 2023. Arctic soil methane sink increases with drier conditions and higher ecosystem respiration. Nat. Clim. Chang. 13, 1095–1104. https://doi.org/10.1038/s41558-023-01785-3.
Walker, K., 2025. tigris: load census TIGER/line shapefiles. R package version 2.2.1.9000. https://github.com/walkerke/tigris.
Wan, S., Norby, R.J., Ledford, J., Weltzin, J.F., 2007. Responses of soil respiration to elevated CO2, air warming, and changing soil water availability in a model old-field grassland. Glob. Chang. Biol. 13, 2411–2424. https://doi.org/10.1111/j.1365-2486.2007.01433.x.
Wanyama, I., Pelster, D.E., Butterbach-Bahl, K., Verchot, L.V., Martius, C., Rufino, M.C., 2019. Soil carbon dioxide and methane fluxes from forests and other land use types in an African tropical montane region. Biogeochemistry 143, 171–190. https://doi.org/10.1007/S10533-019-00555-8.
Wickham, H., Averick, M., Bryan, J., Chang, W., McGowan, L.D., François, R., Grolemund, G., Hayes, A., Henry, L., Hester, J., Kuhn, M., Pedersen, T.L., Miller, E., Bache, S.M., Müller, K., Ooms, J., Robinson, D., Seidel, D.P., Spinu, V., Takahashi, K., Vaughan, D., Wilke, C., Woo, K., Yutani, H., 2019. Welcome to the {tidyverse}. J. Open Source Softw. 4, 1686. https://doi.org/10.21105/joss.01686.
Wickham, H., Bryan, J., 2025. feadxl: read excel files. R package version 1.4.5. https://readxl.tidyverse.org. https://github.com/tidyverse/readxl.
Wickham, H., Henry, L., 2025. purrr: functional programming tools. R package version 1.2.1. https://purrr.tidyverse.org/.
Wickham, H., Pedersen, T.L., Seidel, D., 2023. scales: scale functions for visualization.
Wilson, R.M., Tfaily, M.M., Kolton, M., Johnston, E.R., Petro, C., Zalman, C.A., Hanson, P.J., Heyman, H.M., Kyle, J.E., Hoyt, D.W., Eder, E.K., Purvine, S.O., Kolka, R.K., Sebestyen, S.D., Griffiths, N.A., Schadt, C.W., Keller, J.K., Bridgham, S. D., Chanton, J.P., Kostka, J.E., 2021. Soil metabolome response to whole-ecosystem warming at the spruce and peatland responses under changing environments experiment. Proc. Natl. Acad. Sci. U.S.A. 118, e2004192118. https://doi.org/10.1073/PNAS.2004192118.
Wood, T.E., Tucker, C., Alonso-Rodríguez, A.M., Loza, M.I., Grullón-Penkova, I.F., Cavaleri, M.A., O'Connell, C.S., Reed, S.C., 2025. Warming induces unexpectedly high soil respiration in a wet tropical forest. Nat. Commun. 16, 1–9. https://doi.org/10.1038/S41467-025-62065-6, 2025 16:1.
Wu, X., Yao, Z., Brüggemann, N., Shen, Z.Y., Wolf, B., Dannenmann, M., Zheng, X., Butterbach-Bahl, K., 2010. Effects of soil moisture and temperature on CO2 and CH4 soil–atmosphere exchange of various land use/cover types in a semi-arid grassland in Inner Mongolia, China. Soil. Biol. Biochem. 42, 773–787. https://doi.org/10.1016/J.SOILBIO.2010.01.013.
Xiong, K., Feng, Y., Jin, H., Liang, S., Yu, K., Kuang, X., Wan, L., 2023. A new model to predict soil thermal conductivity. Sci. Rep. 13, 10684. https://doi.org/10.1038/s41598-023-37413-5.
Yaffar, D., Wood, T.E., Reed, S.C., Branoff, B.L., Cavaleri, M.A., Norby, R.J., 2021. Experimental warming and its legacy effects on root dynamics following two hurricane disturbances in a wet tropical forest. Glob. Chang. Biol. 27, 6423–6435. https://doi.org/10.1111/gcb.15870.
Yang, H., Liu, S., Li, Y., Xu, H., 2017. Diurnal variations and gap effects of soil CO2, N2O and CH4 fluxes in a typical tropical montane rainforest in Hainan Island, China. Ecol. Res. 33, 379–392. https://doi.org/10.1007/S11284-017-1550-4, 2017 33:2.
Zhao, J.F., Peng, S.S., Chen, M.P., Wang, G.Z., Cui, Y., Bin, Liao, L.G., Feng, J.G., Zhu, B., Liu, W.J., Yang, L.Y., Tan, Z.H., 2019. Tropical forest soils serve as substantial and persistent methane sinks. Sci. Rep. 9, 1–9. https://doi.org/10.1038/S41598-019-51515-z.
Zhuang, Q., Chen, M., Xu, K., Tang, J., Saikawa, E., Lu, Y., Melillo, J.M., Prinn, R.G., McGuire, A.D., 2013. Response of global soil consumption of atmospheric methane to changes in atmospheric climate and nitrogen deposition. Glob. Biogeochem. Cycles 27, 650–663. https://doi.org/10.1002/GBC.20057.
Zimmerman, J.K., Willig, M.R., Hernández-Delgado, E.A., 2020. Resistance, resilience, and vulnerability of social-ecological systems to hurricanes in Puerto Rico. Ecosphere 11. https://doi.org/10.1002/ECS2.3159.